

1 **Organic enrichment in droplet residual particles relative to out of cloud over the northwest**
2 **Atlantic: Analysis of airborne ACTIVATE data**

3
4 Hossein Dadashazar¹, Andrea F. Corral¹, Ewan Crosbie^{2,3}, Sanja Dmitrovic⁴, Simon Kirschler^{5,6},
5 Kayla McCauley⁷, Richard Moore², Claire Robinson^{2,3}, Joseph S. Schlosser¹, Michael Shook², K.
6 Lee Thornhill², Christiane Voigt^{5,6}, Edward Winstead^{2,3}, Luke Ziemba², Armin Sorooshian^{1,4,7}

7
8 ¹Department of Chemical and Environmental Engineering, University of Arizona, Tucson, AZ,
9 USA

10 ²NASA Langley Research Center, Hampton, VA, USA

11 ³Science Systems and Applications, Inc., Hampton, VA, USA

12 ⁴James C. Wyant College of Optical Sciences, University of Arizona, Tucson, AZ, USA

13 ⁵Institute of Atmospheric Physics, German Aerospace Center

14 ⁶Institute of Atmospheric Physics, University Mainz, Germany

15 ⁷Department of Hydrology and Atmospheric Sciences, University of Arizona, Tucson, AZ, USA

16
17
18 *Correspondence to: Hossein Dadashazar (hosseind@arizona.edu)

19

20

21

22

23 **Abstract.**

24 Cloud processing is known to generate aerosol species such as sulfate and secondary
25 organic aerosol, yet there is a scarcity of airborne data to examine this issue. The NASA Aerosol
26 Cloud meTeorology Interactions oVer the western ATlantic Experiment (ACTIVATE) was
27 designed to build an unprecedented dataset relevant to aerosol-cloud interactions with two
28 coordinated aircraft over the northwest Atlantic, with aerosol mass spectrometer data used from
29 four deployments between 2020-2021 to contrast aerosol composition below, in (using a
30 counterflow virtual impactor), and above boundary layer clouds. Consistent features in all time
31 periods of the deployments (January-March, May-June, August-September) include the mass
32 fraction of organics and relative amount of oxygenated organics (m/z 44) relative to total organics
33 (f_{44}) increasing in droplet residuals relative to below and above cloud. Detailed analysis comparing
34 data below and in cloud suggests a possible role for in-cloud aqueous processing in explaining
35 such results; an intriguing aspect though requiring more attention is that only approximately a
36 quarter of the cloud cases (29 of 110) showed higher organic mass fractions either below or above
37 cloud. Of those 29 cases, the majority (25) showed higher organic mass fraction below cloud base
38 where the cloud processing signature is presumably more evident as compared to above cloud.
39 These results are consistent with the few past studies analyzing droplet residuals pointing to higher
40 organic enrichment than in adjacent cloud-free areas. The data findings are important as other
41 datasets (e.g., reanalysis) suggest that sulfate is both more abundant than organics (in contrast to
42 this work) and more closely related to drop number concentrations in the winter when aerosol-
43 cloud interactions are strongest; here we show that organics are more abundant than sulfate in the
44 droplet residuals and that aerosol interaction with clouds potentially decreases particle
45 hygroscopicity due to the increase in organic:sulfate ratio for droplet residuals relative to
46 surrounding cloud-free air. These results are important in light of the growing importance of
47 organics over the northwest Atlantic in recent decades relative to sulfate owing to the success of
48 regulatory activity over the eastern United States to cut sulfur dioxide emissions.

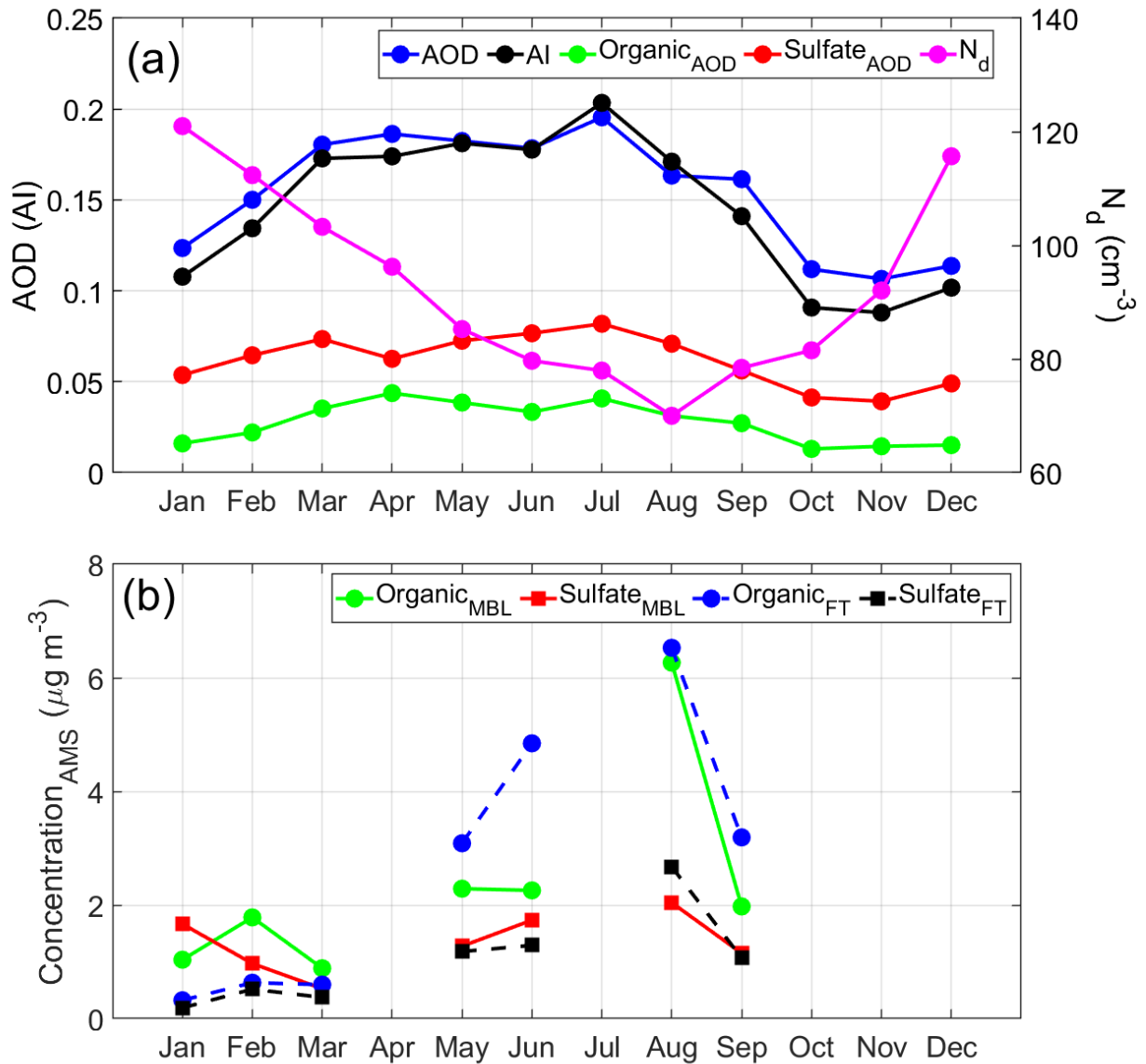
49

50 1. Introduction

51 The nature of aerosol-cloud interactions over the northwest Atlantic Ocean is uncertain
52 even though the region has been the target of decades of atmospheric research (Sorooshian et al.,
53 2020). These interactions include a subset of aerosol particles called cloud condensation nuclei
54 (CCN) that activate into cloud droplets, which subsequently undergo aqueous processing to
55 transform into a particle after evaporation varying in size and composition relative to the original
56 CCN. An aspect of these steps that is poorly characterized is the composition of the droplet
57 residuals in cloud relative to particles below and above clouds, which requires airborne
58 measurements. The NASA Aerosol Cloud meteorology Interactions over the western Atlantic
59 Experiment (ACTIVATE) was designed to collect in situ and remote sensing data in and around
60 clouds during different seasons in a region with a wide range of weather conditions (Painemal et
61 al., 2021) and air mass sources (Corral et al., 2021), qualifying as a suitable dataset to examine
62 this very issue.

63 The annual cycle of aerosol and cloud drop number concentrations (N_d) varies in the
64 northwest Atlantic, with aerosol parameters (e.g., aerosol optical depth, aerosol index) peaking in
65 summer months in contrast to N_d being highest the winter (Figure 1). This discrepancy was
66 reconciled by Dadashazar et al. (2021a) who showed that conditions linked to cold air outbreak
67 events (e.g., enhanced turbulence, higher marine boundary layer (MBL) height, higher low-level
68 liquid cloud fraction) promote stronger aerosol-cloud interactions in the winter to help activate
69 particles into drops with higher efficiency than other times of the year. Gradient boosted regression
70 tree analysis revealed that the most influential aerosol parameter in predicting N_d was either surface
71 mass concentration of sulfate (winter) or organics (summer). However, those results were based
72 on reanalysis data without any indication of causal effects between aerosol composition and cloud
73 microphysics. Airborne in situ data are needed to unravel the composition details in and around
74 clouds. Of particular interest related to aerosol chemical characterization around clouds is growing
75 evidence in the literature that in-cloud aqueous processing can generate not only sulfate (Barth et
76 al., 2000; Ervens, 2015) but also secondary organic aerosol (SOA) (Blando and Turpin, 2000;
77 Warneck, 2003; Sorooshian et al., 2006a; Ervens et al., 2011; Heald et al., 2011), which is
78 hypothesized to manifest itself in enhanced organic mass fractions in droplet residuals relative to
79 below and above cloud. Past work over the northwest Atlantic has pointed to the importance of
80 secondary formation via gas-to-particle conversion processes in influencing the organic carbon
81 budget of aerosol particles (de Gouw et al., 2005; Schroder et al., 2018; Shah et al., 2019).
82 Furthermore, chemical analysis of droplet residuals should lend insight into the properties of
83 aerosol particles that will be released after droplets evaporate, which could control their propensity
84 to activate in a subsequent passage through cloud, with past work showing an important role for
85 organics (Russell et al., 2000; Drewnick et al., 2007; Mertes et al., 2007; Hawkins et al., 2008;
86 Asa-Awuku et al., 2015).

87 The goal of this study is to compare aerosol mass spectrometer data over the northwest
88 Atlantic below, in, and above clouds for different times of the year (January-March, May-June,
89 August-September). Case studies of flights during cold air outbreaks probe deeper to better
90 understand the nature of aerosol and droplet residual particle composition during these events with
91 stronger aerosol-cloud interactions as compared to other times of the year (Dadashazar et al.,
92 2021a; Painemal et al., 2021). The results have implications for aerosol-cloud interactions as
93 droplet residual composition is shown here to deviate from that of aerosol out of cloud.



94

95 **Figure 1. (a) Monthly mean values (January 2013 – December 2017) of CERES-MODIS**
 96 **cloud droplet number concentration (N_d) for low-level clouds (heights below 700 hPa),**
 97 **MERRA-2 aerosol index, and MERRA-2 total and speciated (sulfate and organic) aerosol**
 98 **optical depth. Data used apply to the spatial area over the northwest Atlantic where**
 99 **ACTIVATE data were collected (boxes 1-3 in Figure 2). (b) Monthly mean values of sulfate**
 100 **and organic using ACTIVATE airborne data differentiated by marine boundary layer**
 101 **(BCB/BBL legs) versus free troposphere (ACT/ABL legs); these legs are described in Section**
 102 **2.1.**

103

104 2. Methods

105 2.1 Field Campaign Description

106 We use airborne in situ data collected aboard the HU-25 Falcon from deployments 1 (14
107 February – 12 March 2020), 2 (13 August – 30 September 2020), 3 (27 January – 2 April 2021),
108 and 4 (13 May – 30 June 2021) of the ACTIVATE mission. Data necessary for this study were
109 only available for two flights in deployment 3 (29 January and 3 February) owing to an aircraft
110 maintenance issue reducing the size of the available payload. ACTIVATE employs a dual aircraft
111 approach with the Falcon acquiring in situ data for trace gases, aerosol particles, and clouds in the
112 MBL while a King Air flies overhead at ~9 km conducting remote sensing measurements and
113 launching dropsondes (Sorooshian et al., 2019). Typical flights are ~3-4 hours based out of NASA
114 Langley Research Center in Hampton, Virginia. The Falcon flies in what are termed “ensembles”,
115 which comprise legs in the following nominal order: below cloud base (BCB), above cloud base
116 (ACB), BCB, ACB, minimum altitude leg at ~150 m (Min. Alt.), above cloud top (ACT), below
117 cloud top (BCT), and then descent back to BCB to start a new ensemble. Cloud-free ensembles
118 include the following legs: Min. Alt., below boundary layer top (BBL), above boundary layer top
119 (ABL), and then descent back down to Min. Alt. to start a new ensemble. The Falcon flies at ~120
120 m s⁻¹, with the duration (length) of each leg and cloud ensemble being ~3.3 min (~24 km) and 35
121 min (~250 km), respectively. Cloud-free ensembles were approximately 15 min (~100 km). The
122 repeated nature of these ensembles has built a large statistical database relevant to aerosol-cloud-
123 meteorology interactions. Clear ensembles were generally closer to the coast.

124

125 **2.2 Airborne Instrument Details**

126 The central dataset relevant to aerosol composition in this study comes from the Aerodyne
127 High-Resolution Time-of-Flight Aerosol Mass Spectrometer (AMS) (DeCarlo et al., 2008). The
128 instrument measures submicrometer non-refractory aerosol composition in 1 Hz Fast-MS mode
129 with data averaged to 25-second time resolution. We make use of specific mass spectral markers
130 including m/z 43 (mostly C₂H₃O⁺) and 44 (CO₂⁺), which represent oxygenated organic fragments,
131 with the ratios of the markers relative to total organic mass referred to as f₄₃ and f₄₄, respectively.
132 AMS measurements were conducted downstream of an isokinetic double diffuser inlet (Brechtel
133 Manufacturing Inc.) in cloud-free conditions and downstream of a counterflow virtual impactor
134 (CVI) inlet (Brechtel Manufacturing Inc.) in clouds (Shingler et al., 2012). For classification of
135 data as cloud and cloud-free, we use a liquid water content (LWC) threshold of 0.05 g m⁻³ based
136 on data from the Fast Cloud Droplet Probe (FCDP; D_p ~3 – 50 μm) (SPEC Inc.; Kirschler et al.,
137 2022). This LWC threshold has been used in recent work using ACTIVATE data (Dadashazar et
138 al., 2021a). Data for both rain water content and ice water content were used from a two-
139 dimensional stereo probe vertical direction (2DS-V; D_p ~29 – 1465 μm) (SPEC, Inc.). We also use
140 a proxy for hygroscopicity in the form of f(RH), which is the ratio of total light scattering between
141 relative humidities of 80% and 20% as measured by tandem nephelometers (TSI Inc, St. Paul, MN,
142 USA; Model 3563) (Ziamba et al., 2013).

143 Note that while cloud water samples were also chemically characterized, those data are
144 outside the scope of this work as the partial speciation of organics in the cloud water samples
145 makes it hard to compare to AMS total organics. Furthermore, particle-into-liquid sampler (PILS)
146 data are not used owing to lengthier time resolution (~5 min) and chemical smearing during sample
147 collection (Sorooshian et al., 2006b) preventing a clear assignment of data to individual legs in
148 ensembles.

149

150 **2.3 Complementary Datasets**

151 **2.3.1 HYSPLIT and CWT Maps**

152 We obtained 5-day back-trajectory data from NOAA’s Hybrid Single-Particle Lagrangian
153 Integrated Trajectory (HYSPLIT) model (Stein et al., 2015; Rolph, 2017) ending at the Falcon
154 position during any of the 29,164 cloud-free AMS data points. Note that this includes data during
155 cloud ensembles but only when cloud liquid water content was $< 0.05 \text{ g m}^{-3}$, and thus data during
156 BCB and ACT legs are included. We relied on the National Centers for Environmental
157 Prediction/National Center for Atmospheric Research (NCEP/NCAR) reanalysis data using the
158 “Model vertical velocity” method and obtained data points every 6 hours along trajectories.

159 As this study is mainly focused on organics and sulfate, concentration-weighted trajectory
160 (CWT) maps were generated using HYSPLIT back-trajectories in conjunction with speciated AMS
161 data (Figures S1-S2) to show the predominant sources for each of these two aerosol components
162 (e.g., Hsu et al., 2003). As demonstrated by past works for other regions (e.g., Dadashazar et al.,
163 2019), the method assigns a weighted concentration to grid cells based on mean concentrations
164 passing through each grid cell from all the considered trajectories. CWT profile maps are produced
165 using the GIS-based software called TrajStat (Wang et al., 2009).

166 **2.3.2 MERRA-2**

167 We use both total and speciated (sulfate and organic) aerosol optical depth (AOD) at 550
168 nm from the Modern-Era Retrospective analysis for Research and Applications-Version 2
169 (MERRA-2) (Gelaro et al., 2017) between January 2013 and December 2017 near Aqua’s overpass
170 time (13:30 local time). We also show results for aerosol index (AI), which is the product of AOD
171 and the Ångström parameter. As the latter accounts for aerosol size, AI is better related to columnar
172 CCN as compared to AOD (Nakajima et al., 2001). Data are used for the spatial area over the
173 northwest Atlantic where ACTIVATE data were collected (boxes 1-3 in Figure 2).

174 **2.3.3 CERES-MODIS**

175 Cloud droplet number concentrations (N_d) are presented for the ACTIVATE region
176 following the specific calculations and filtering methods of Dadashazar et al. (2021a) using Clouds
177 and the Earth’s Radiant Energy System (CERES) edition 4 products (Minnis et al., 2011; Minnis
178 et al., 2021). CERES retrieval algorithms are applied to MODerate resolution Imaging
179 Spectroradiometer (MODIS)-Aqua radiances as obtained during daytime overpasses around 13:30
180 local time. Level 3 cloud data were used between January 2013 and December 2017 at $1^\circ \times 1^\circ$
181 resolution for low-level clouds ($> 700 \text{ hPa}$) based on CERES-MODIS edition 4 Single Scanning
182 Footprint (SSF) products (Loeb et al., 2016). N_d was calculated with an adiabatic cloud model
183 (Grosvenor et al., 2018):

184

$$185 \quad N_d = \frac{\sqrt{5}}{2 \pi k} \left(\frac{f_{ad} C_w \tau}{Q_{ext} \rho_w r_e^5} \right)^{1/2} \quad (1)$$

186

187 where k represents the droplet spectrum width (assumed to be 0.8 over the ocean), r_e is cloud drop
188 effective radius, τ is cloud optical depth, Q_{ext} is the unitless extinction efficiency factor (assumed
189 to be 2 for liquid droplets), and ρ_w is the density of water (1 g cm^{-3}). N_d data are used when low-
190 level liquid cloud fraction exceeded 40%. Data are used for the same spatial area as MERRA-2
191 data (i.e., boxes 1-3 in Figure 2).

192

193 **2.4 Classification of Cold Air Outbreak Flights**

194 We determine whether flights occurred during cold air outbreaks (CAOs) leveraging
195 methods in recent ACTIVATE studies (Seethala et al., 2021; Corral et al., 2022). Briefly, Visible
196 Infrared Imaging Radiometer Suite (VIIRS) imagery (NASA Worldview) is used to visually
197 identify cloud streets that are characteristic of CAOs. Flight notes and weather forecast slides were
198 used as additional confirmation, followed by data from dropsondes released from the King Air
199 following the method described in Papritz et al. (2015).

200

201 **3. Results**

202 A motivation of this study is the opposite annual pattern of N_d and aerosol parameters
203 shown in Figure 1a. Notable is that sulfate AOD exceeds that of organic AOD for all months based
204 on MERRA-2 data, which has been shown before in the region (Braun et al., 2021). The
205 ACTIVATE airborne data show that while the total concentrations of both aerosol components are
206 higher in the summer months (similar to related aerosol parameters in Figure 1a), a difference
207 compared to MERRA-2 speciated AODs is that organic levels exceed those of sulfate (except
208 January in the MBL), regardless of whether the data were collected in the MBL (i.e., BBL and
209 BCB legs) or free troposphere (i.e., ACT and ABL legs) (Figure 1b). Hegg et al. (1997) concluded
210 for the month of June based on a chemical apportionment study using aerosol column optical depth
211 data off the mid-Atlantic coast of the United States that the three most abundant components (in
212 decreasing order) were water, carbonaceous compounds, and then sulfate. This is an important
213 result with implications for aerosol characteristics such as hygroscopicity. For instance, higher
214 organic:sulfate mass ratios in the MBL correspond to suppressed hygroscopic growth factors at
215 high relative humidities ($\geq 85\%$) (Hersey et al., 2009).

216

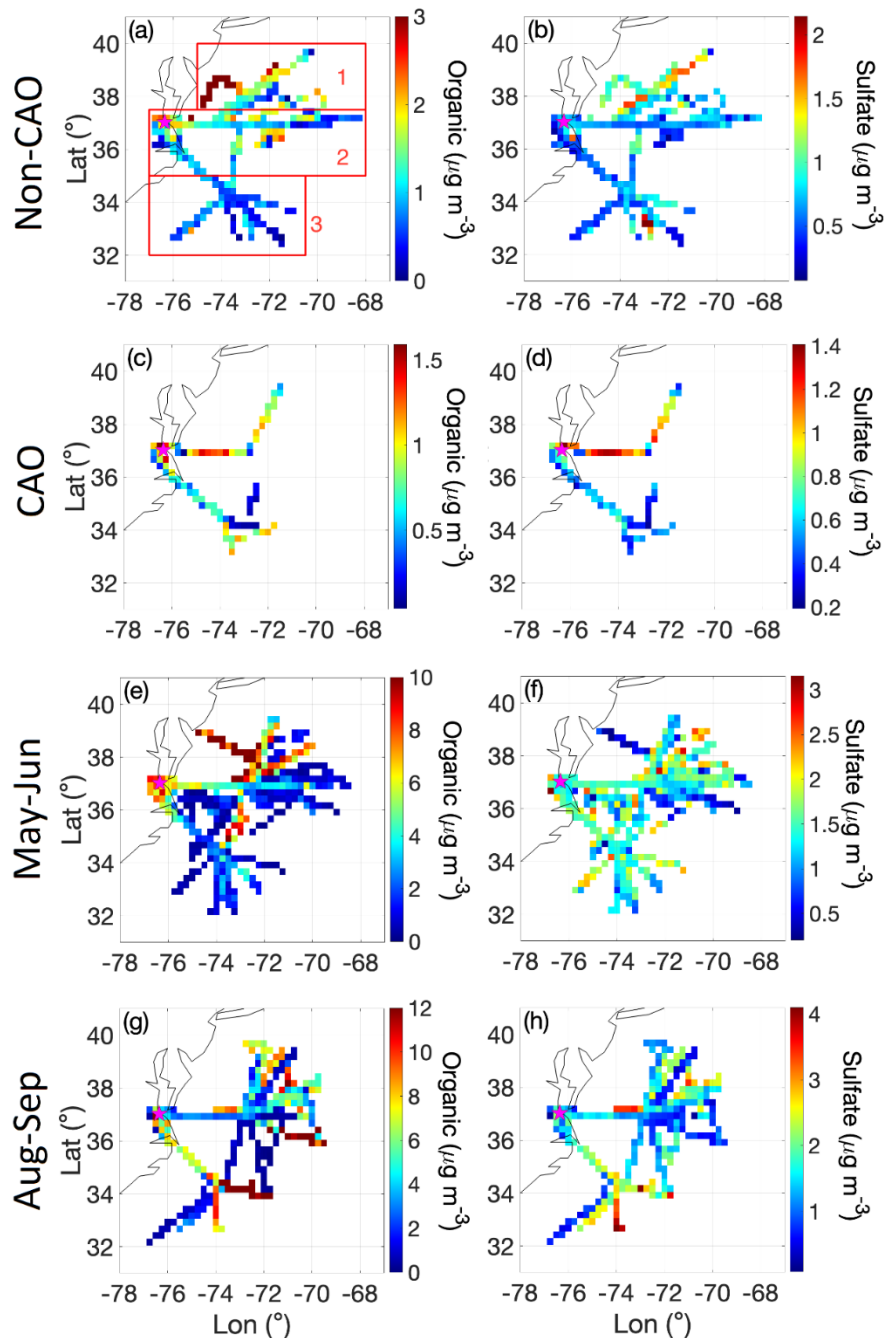
217 **3.1 Multi-season Overview of AMS Composition**

218 Relative to all AMS species, sulfate and organics are the dominant aerosol components by
219 mass with combined mass fractions being near 75% usually regardless of season or location
220 relative to clouds (Tables S1-S2; spatial maps in Figure 2); this is consistent with their predictive
221 capability for N_d over the northwest Atlantic (Dadashazar et al., 2021a). Nitrate and ammonium
222 were the next most abundant components. The highest organic concentrations were in August-
223 September assisted in part by transported wildfire emissions from western North America (Mardi
224 et al., 2021). Mean vertical profiles of organics in each season (Figure 3) show that in all months,

225 but especially May-June and August-September, there is an enhancement at altitudes exceeding
226 200 m in the northernmost parts of the study region. Organic aerosol CWT maps reveal significant
227 influence from continental sources based on the highest concentrations along trajectories coming
228 from the U.S. East Coast (Figure S1). In terms of the nature of the organic aerosol fraction, vertical
229 profiles of f_{44} were fairly similar between seasons and areas of the study region (Figure 2), ranging
230 in mean value for the various leg types in Table S1 between 0.11 and 0.27. For reference, the f_{44}
231 of atomized oxalic acid, a tracer for cloud processing in the absence of biomass burning and coarse
232 aerosol (Hilario et al., 2021 and references therein), is 0.36 (Lambe et al., 2011).

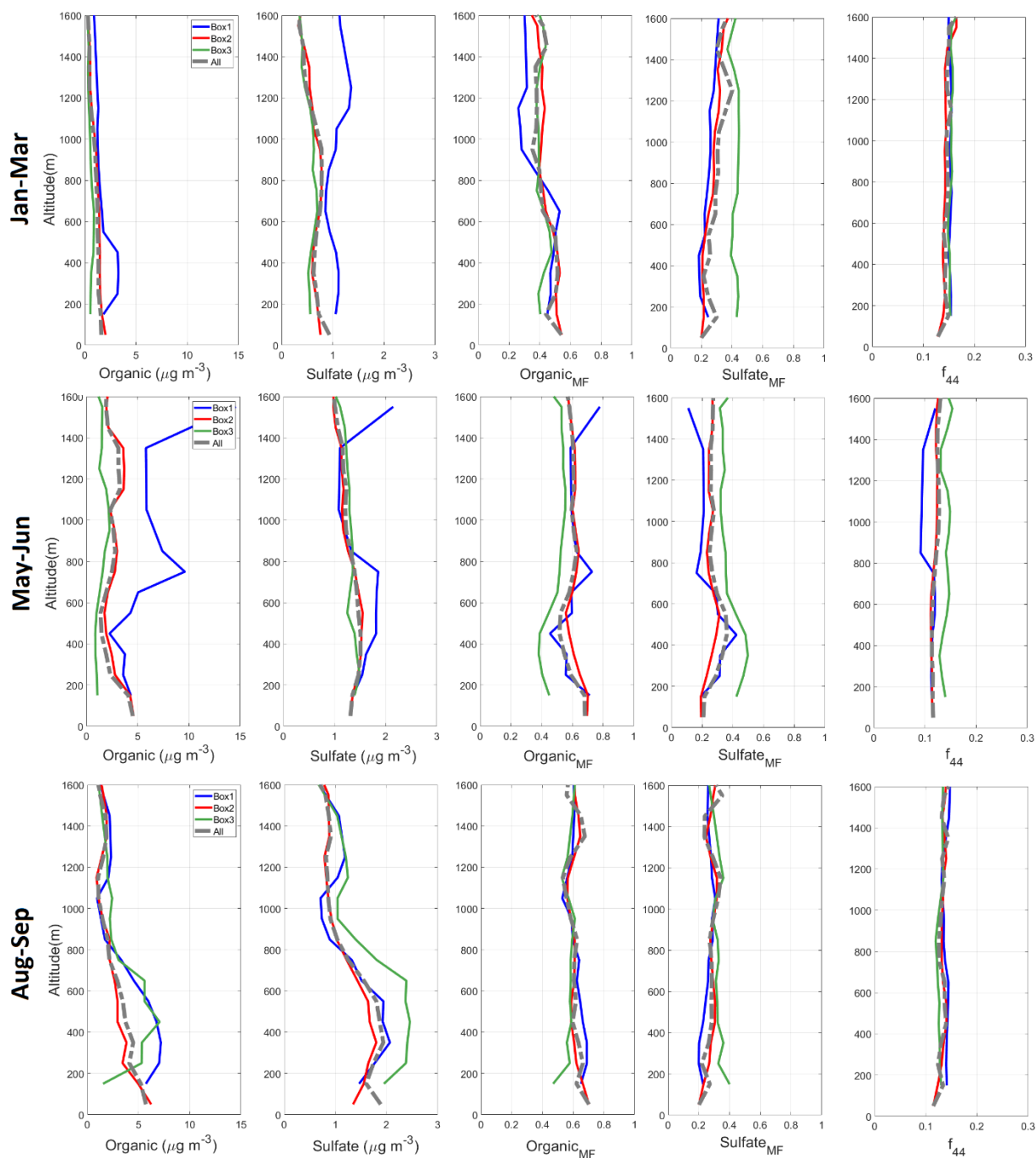
233 In contrast to organics, sulfate exhibits more spatially homogenous concentrations over the
234 northwest Atlantic (Figure 2) owing largely to ocean-emitted dimethylsulfide that undergoes gas
235 and in-cloud oxidation such as what was shown for the eastern North Atlantic (Ovadnevaite et al.,
236 2014). This is supported by how sulfate's seasonal CWT maps (Figure S2) differ from those of
237 organics with comparable concentrations widespread over the northwest Atlantic relative to the
238 continent. The August-September CWT map for sulfate reveals more high concentration areas
239 (note the different color bar scale for Aug-Sep in Figure S2) over the continent with concentrations
240 exceeding those over most of the ocean; this is presumably due to more secondary formation
241 stemming from local sulfur dioxide emissions over the eastern U.S. (Yang et al., 2018) aided in
242 part by higher temperatures and humidity (Corral et al., 2021) that co-vary with other conditions
243 favorable for sulfate production such as stagnation and certain air flow patterns (Tai et al., 2010).
244 Figure 3 demonstrates that neither sulfate or organics exhibit a clear reduction with altitude
245 pointing towards a potential source aloft that might include long-range transport and/or secondary
246 production.

247 Although based on only two consecutive days of flight data, results from Leaitch et al.
248 (2010) are relevant in that they sampled below, in, and above boundary layer clouds over the
249 northwest Atlantic. On the first day with more marine influence, sulfate was more abundant than
250 organics in fine particles below cloud. In contrast, the second day had more continental influence
251 with organic levels exceeding those of sulfate below cloud, which was often the case during
252 ACTIVATE (Table S1). They concluded with a parcel model that the impact of anthropogenic
253 carbonaceous components on the cloud albedo effect can exceed that of anthropogenic sulfate,
254 which motivates attention to the droplet residual composition discussed next.



255

256 **Figure 2. Spatial map of cloud-free AMS data for organics and sulfate collected during**
 257 **deployments 1-4 of ACTIVATE spanning from February 2020 to June 2021. Non-CAO and**
 258 **CAO represent non-cold air outbreak and cold air outbreak days, respectively, between**
 259 **January and March. Spatial boxes labeled 1-3 in (a) correspond to domains used for**
 260 **calculations in other parts of this study. Grid cells are $0.25^\circ \times 0.25^\circ$ and represent an average**
 261 **of data across all vertical levels flown between 0.02 and 8.1 km. Color bar scales differ by**
 262 **panel to highlight variability better within a panel.**



263

264 **Figure 3. Vertically-resolved cloud-free AMS data for the different time periods of**
 265 **ACTIVATE deployments and boxes defined in Figure 2a. Shown are (left to right) organic**
 266 **and sulfate concentrations, organic and sulfate mass fraction, and the ratio of m/z 44 to**
 267 **total organic (f_{44}). The top row for January-March combines CAO and non-CAO days,**
 268 **which are separated for other parts of the study.**

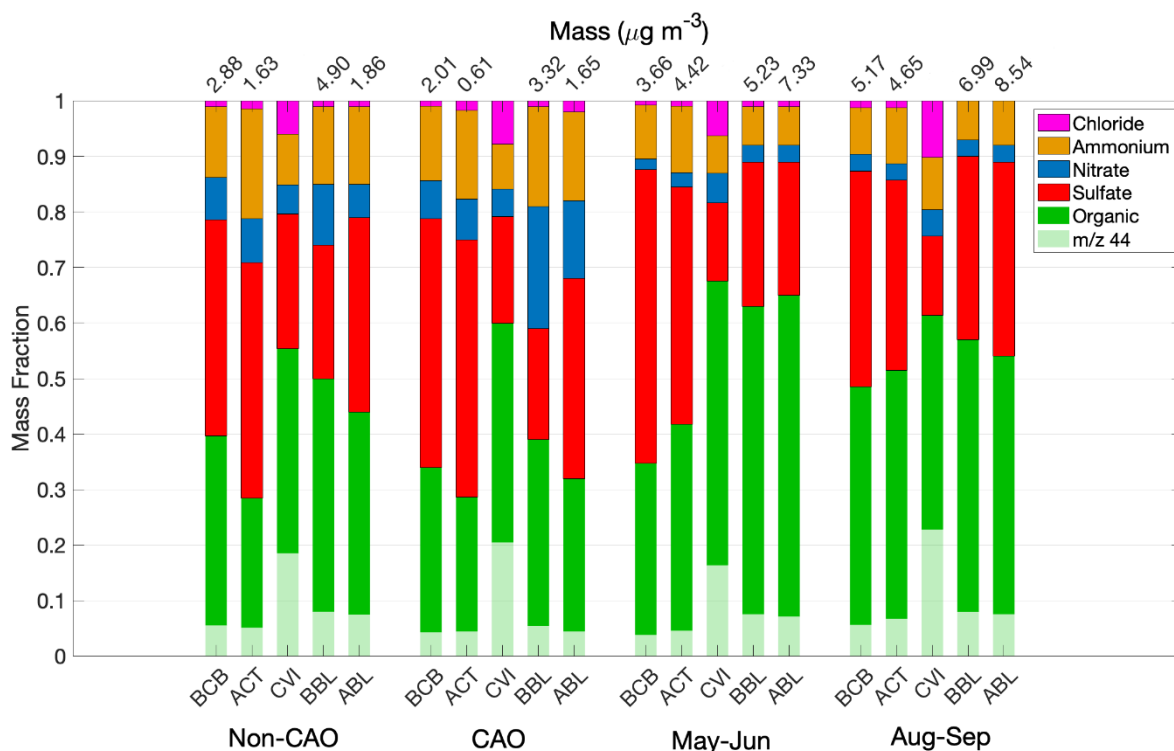
269

270

271 **3.2 Droplet Residual Composition**

272 A striking result in all seasons is that organic mass fraction was higher downstream of the
273 CVI in droplet residual particles in contrast to adjacent BCB and ACT legs in cloud ensembles
274 (Figure 4 and Table S1). To compensate, sulfate mass fractions decreased in droplet residuals.
275 Furthermore, f_{44} increased in droplet residuals as compared to BCB and ACT data in each season,
276 indicative of more contribution of oxygenated organic species like carboxylic acids. There was no
277 significant difference in the mass fraction profiles between seasons for a fixed leg type (Figure 4).
278 The higher organic mass fractions in the BBL/ABL legs of clear ensembles relative to BCB/ACT
279 legs of cloud ensembles can be explained by how most of the clear ensemble data were collected
280 closer to land where there are greater organic levels in the continental outflow relative to farther
281 offshore where sulfate presumably becomes more important due to marine emissions of precursors
282 such as dimethylsulfide. The region's synoptic flow is not always strictly offshore from west-to-
283 east. Thus, the higher organic content near the coast often could just be due to local emissions that
284 are confined to the coast and are not advected any farther east.

285 The organic mass fraction and f_{44} changes in droplet residuals can be explained at least in
286 part by some combination of preferential activation of CCN with these special properties and/or
287 aqueous processing in droplets to generate oxygenated organics. Although not the focus here, the
288 high chloride mass fractions in droplet residuals (Figure 4) can be explained by how sea salt would
289 preferentially activate into drops owing to its large size and that the AMS has some ability (albeit
290 not efficient) to detect sea salt chloride (Zorn et al., 2008; Ovadnevaite et al., 2012).

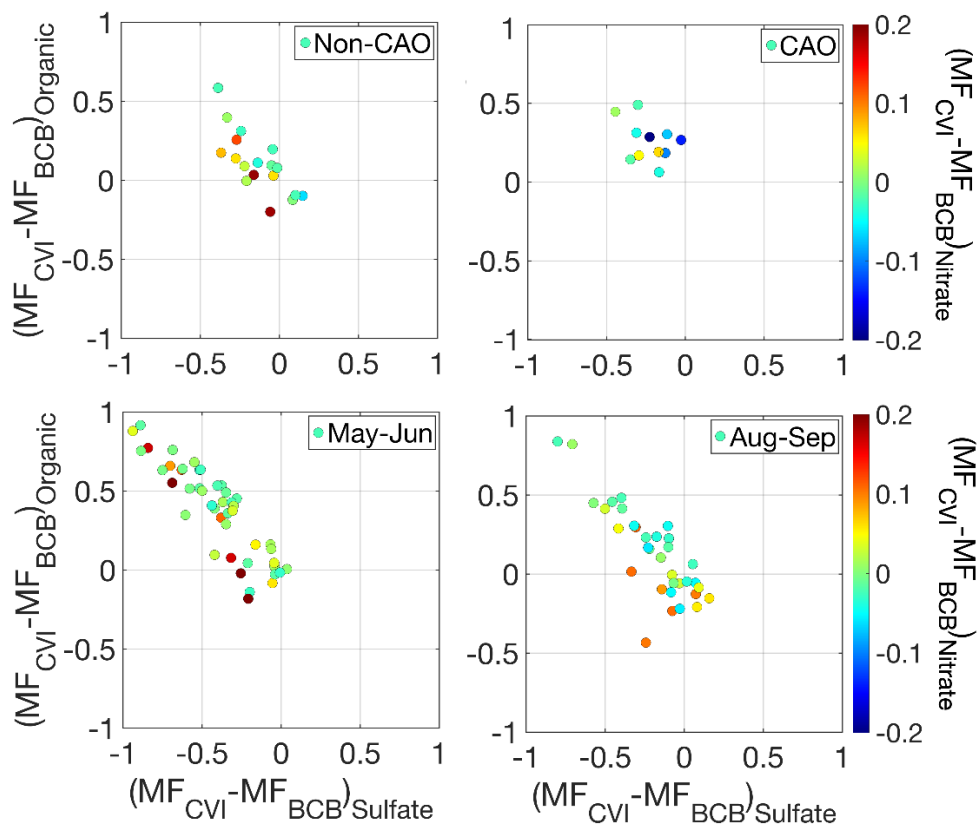


291

292 **Figure 4. Seasonal comparison of AMS mass fractions, including the relative contribution of**
 293 **m/z 44 to total organic (f_{44}). Numbers above each bar represent the mean total AMS mass**
 294 **concentration for that category; note that absolute masses are not reported downstream of**
 295 **a CVI owing to high uncertainties. Note that the Non-CAO and CAO categories represent**
 296 **all flight data in January-March (deployments 1 and 3) that were separated using the criteria**
 297 **in Section 2.4.**

298

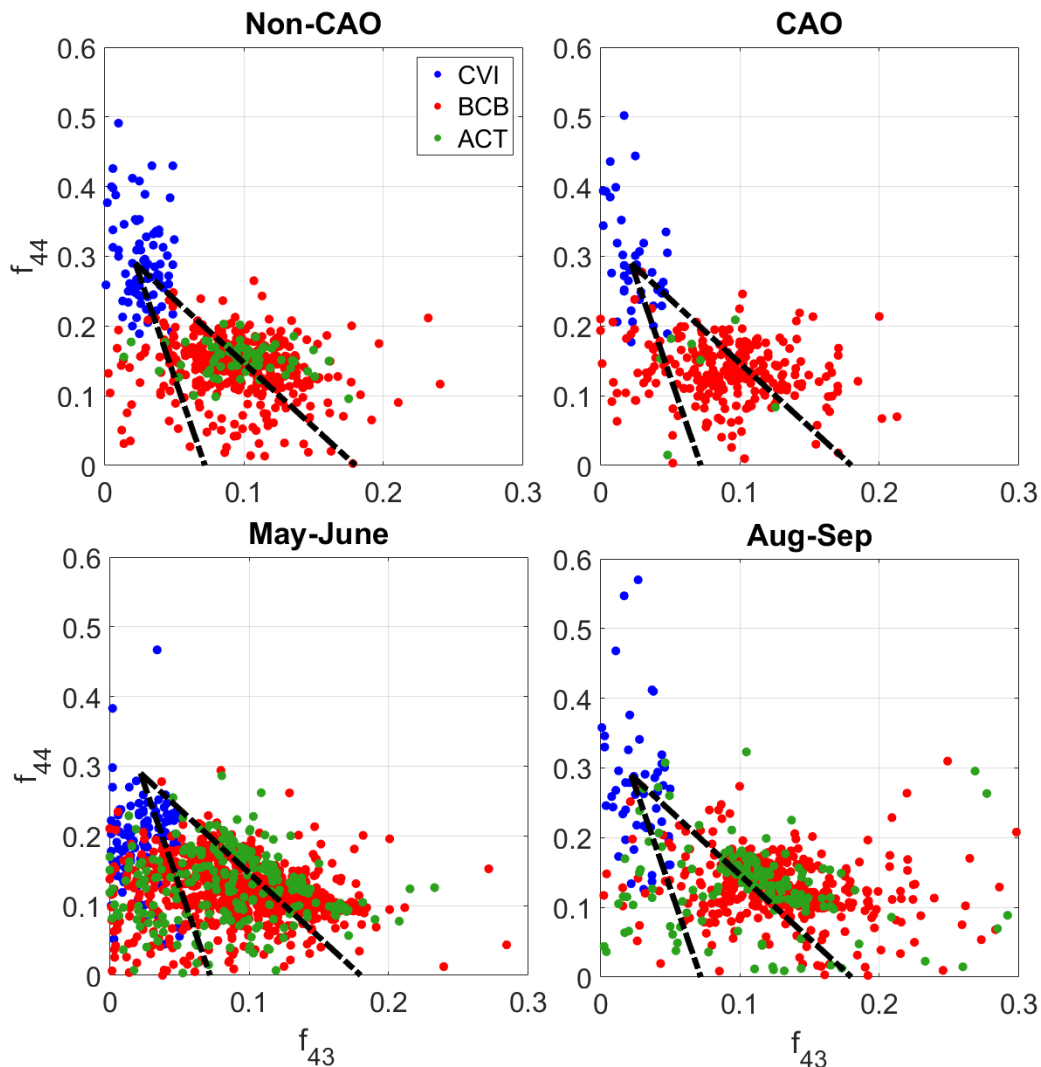
299 We next examine scatterplots of organic mass fraction (i.e., organic mass divided by total
 300 AMS mass) differences between each cloud leg with CVI-AMS data and its closest BCB leg in
 301 the same cloud ensemble versus analogous sulfate mass fraction differences for the same pair of
 302 legs (Figure 5). Aqueous processing to preferentially increase one of the two species relative to
 303 the other would presumably translate into a positive value on the more preferred species' axis; in
 304 other words, if there was more organic aerosol formation in clouds via aqueous processing
 305 relative to sulfate, it would register as a positive (negative) value on the y (x) axis. Regardless of
 306 season, the results reveal a consistent feature of increasing (decreasing) organic (sulfate) mass
 307 fraction downstream of the CVI relative to BCB samples, suggestive of aqueous processing
 308 shifting the composition to be more organic-rich. For the very few points laying to the bottom
 309 left of the origin, nitrate is often more enhanced in those droplet residual samples relative to
 310 BCB data. Comparing CVI-AMS data to the closest ACT leg in the same ensemble reveals a
 311 similar trend (not shown).



312

313 **Figure 5. Scatterplot of the difference in organic mass fraction in cloud legs with CVI data**
 314 **and below cloud base (BCB) legs for an individual cloud ensemble relative to the analogous**
 315 **difference for sulfate mass fraction between the same pair of legs. Markers are colored by**
 316 **the analogous difference in nitrate mass fraction. Panels represent different seasons with**
 317 **winter deployments (January-March) separated into CAO and non-CAO days.**

318 A comparison of f_{44} versus f_{43} in “triangle plot” format (Ng et al., 2010) shows an important
 319 difference between CVI and BCB/ACT data in each season (Figure 6). Ambient organic aerosol
 320 typically converge at the top left of the triangle representative of more atmospheric aging leading
 321 to low volatility oxygenated organic aerosol species. The CVI data are systematically higher and
 322 to the left of the triangle plot in each season. In contrast, the BCB and ACT data are lower and to
 323 the right of the triangle plots without much distinction, suggestive of a similarly lower level of
 324 oxygenation relative to droplet residuals.

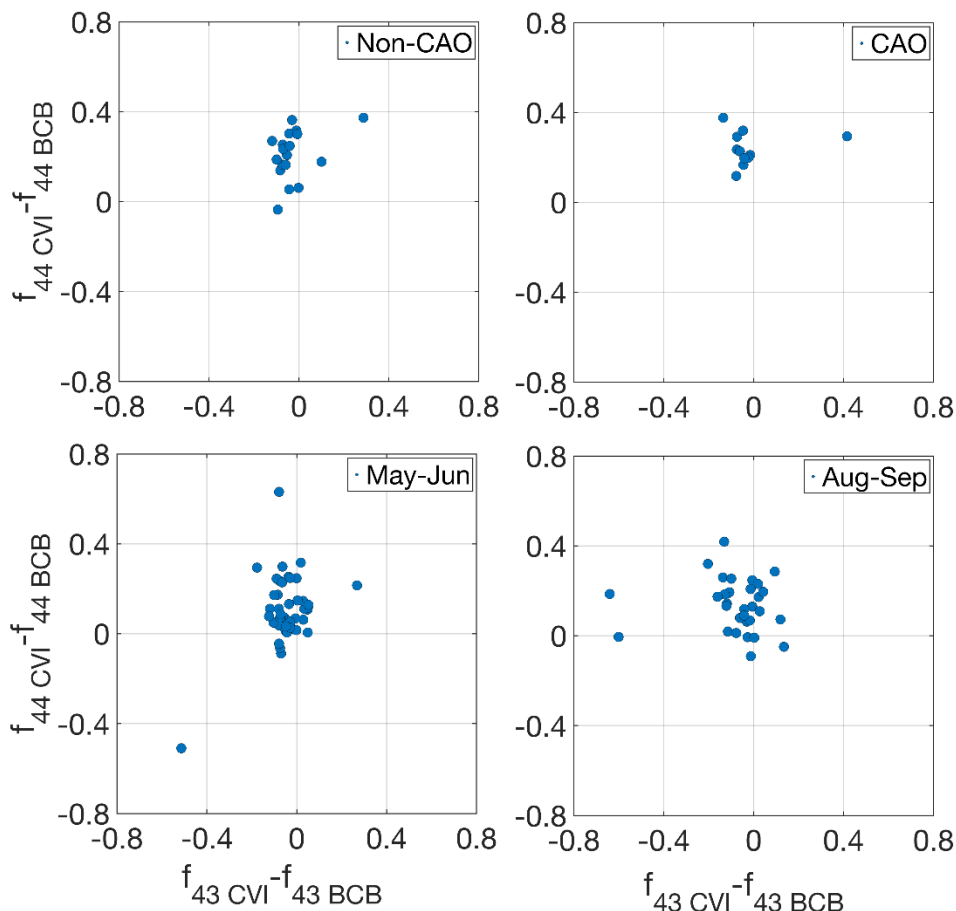


325

326 **Figure 6. Comparison of f_{44} and f_{43} for individual BCB and ACT legs out of cloud, in addition**
 327 **to CVI data in cloud legs. Panels represent different seasons with winter deployments**
 328 **(January-March) separated into CAO and non-CAO days. Superimposed on the plots are**
 329 **triangles corresponding to how former work (Ng et al., 2010) compared these ratios. Points**
 330 **with organic mass concentration less than $0.5 \mu\text{g m}^{-3}$ were omitted from this analysis.**

331 The CVI droplet residuals are more oxidized because of some combination of aqueous
 332 processing effects to yield more oxidized organic species, or because CCN with higher f_{44} activated
 333 into droplets. To probe more into which of the two aforementioned processes could be more
 334 responsible for the cluster of CVI points at the top left of the triangle plots, we next examine
 335 (analogous to Figure 5) scatterplots of $f_{44,\text{CVI}} - f_{44,\text{BCB}}$ versus $f_{43,\text{CVI}} - f_{43,\text{BCB}}$, where data are
 336 compared between the pair of cloud and BCB legs closest to one another in individual cloud
 337 ensembles (Figure 7). If there was no difference in organic composition between a pair of legs,
 338 a marker representing that pair would be at the origin. Aqueous processing is presumed to result in
 339 a positive (negative) value on the y (x) axis. Each season consistently exhibits points positioned

340 to the top left of the origin suggestive of aqueous processing leading to the enhanced oxygenation
 341 of the organic fraction in droplet residuals relative to BCB legs.



342
 343 **Figure 7. Scatterplot of the difference in f_{44} in cloud legs with CVI data and below cloud base**
 344 **(BCB) legs for an individual cloud ensemble relative to the analagous difference for f_{43} .**
 345 **Panels represent different seasons with winter deployments (January-March) separated into**
 346 **CAO and non-CAO days.**

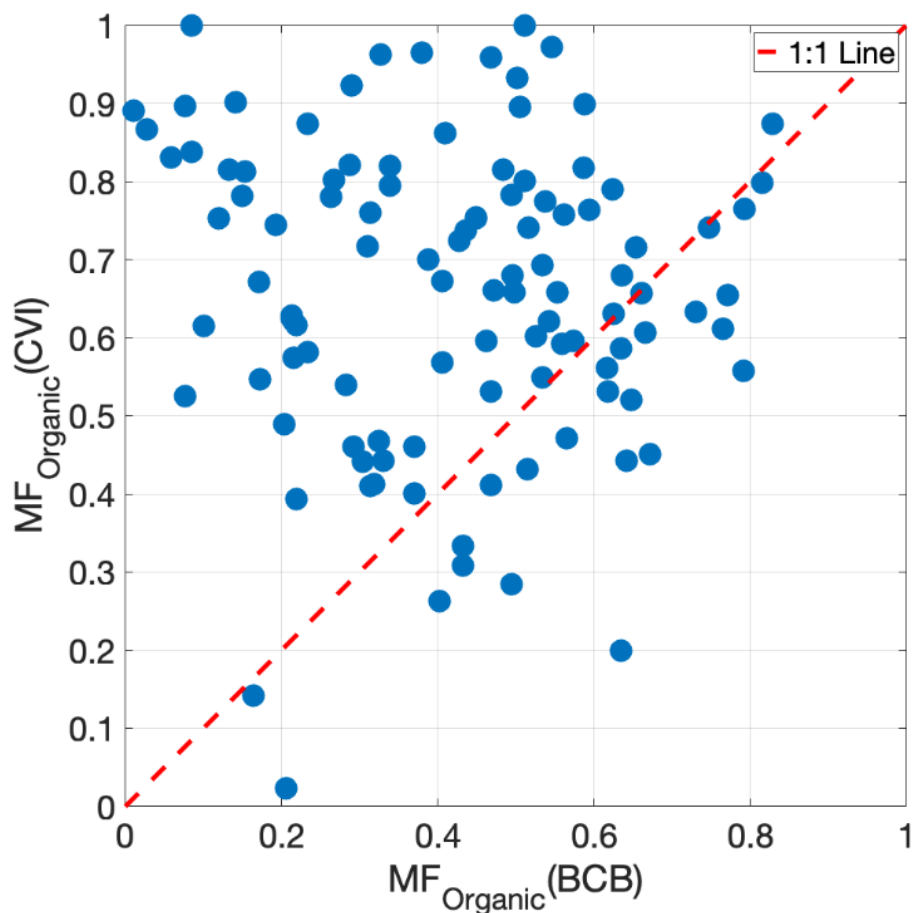
347 A discussion on possible contributing factors (other than aqueous processing) to the
 348 different chemical signature in CVI samples relative to adjacent cloud-free areas is warranted.
 349 First, we note that 23% of BCB/CVI pairs of data points (25 out of 110) exhibited higher organic
 350 mass fraction in the BCB leg relative to droplet residuals (Figure 8). This number increases to 26%
 351 when considering if either the BCB or ACT organic mass fraction was higher than the
 352 corresponding CVI data in cloud for an ensemble. Clearly the cases where a higher organic mass
 353 fraction was observed out of cloud seems to be most prevalent below cloud suggesting that location
 354 is where a cloud processing signature can be more reliably observed. These 26% of the cases
 355 studied demonstrate that the null case exists without an organic enhancement downstream of the
 356 CVI, reducing concerns over instrument and sampling artifacts.

357 In terms of the contamination due to the inlet's material of construction, the CVI inlet was
358 designed with both stainless steel and aluminum yielding negligible organic contamination
359 (Shingler et al., 2012). A way to test this is to conduct CVI sampling in cloud-free conditions.
360 Figure S3 shows a representative time series of AMS data during a flight (research flight 10 on 28
361 February 2020) with numerous cloud passes and periods when there was still sampling
362 downstream of the CVI inlet outside of cloud. During those three key periods shown out of cloud
363 with CVI sampling, sulfate and organic levels exhibit concentrations close to zero and with
364 concentrations considerably lower than CVI data in cloud. Compared to sulfate, there is more
365 variability in organic levels downstream of the CVI regardless of whether sampling was in or out
366 of cloud or even whether sampling was done using the isokinetic inlet out of cloud. The data reveal
367 that at small time scales there is variability in the organic:sulfate ratio behind the CVI in cloud,
368 specifically when comparing the clouds at 16:18-16:29 versus 16:39-16:43 with the former being
369 more organic rich. This representative time series provides confidence in the inlet itself not being
370 the source of the significant changes observed downstream the CVI throughout the first four
371 ACTIVATE deployments. This case flight is examined more in Section 3.3.

372 The heated counterflow in the CVI reduces positive artifacts from volatile gaseous species
373 partitioning into sampled droplets such as with volatile organic compounds (VOCs) to form
374 organics or with nitric acid to form nitrate (Prabhakar et al., 2014); in contrast, the heated
375 counterflow would presumably evaporate some fraction of the existing nitrate and organics in the
376 CCN that activated into droplets unlike sulfate which is not volatile. Thus, the heated inlet would
377 tend to favor sulfate in the cloud droplet residuals and could not explain the enhanced organic
378 residual observations here.

379 Inlets including the CVI can be prone to droplet shatter such as with large drizzle drops (>
380 100 μm) (Twohy et al., 2013), although drizzle was not always frequent and the particulate artifacts
381 generated would still be representative of droplet residuals. It seems implausible that such drop
382 shatter would lead to an organic enrichment especially as the chemical results we report were
383 consistent across the entire study region. AMS results were compared to both rain water content
384 and ice water content without evidence of a distinct relationship between precipitation levels and
385 whether or not there was a higher organic mass fraction behind the CVI relative to out of cloud.

386 It is also noteworthy that there can be considerable variability in AMS composition along
387 level legs (BCB, in cloud, ACT) pointing to how a signature of cloud processing out of cloud can
388 be reduced when averaging data. Figure S3 demonstrates variability along individual legs that is
389 not consistent with the organic:sulfate ratio always being enhanced downstream of the CVI.



390

391 **Figure 8. Scatterplot of organic mass fraction in droplet residuals (downstream CVI in**
 392 **cloud) and in aerosol sampled during the closest below cloud base (BCB) leg from**
 393 **ACTIVATE deployments 1-4. A total of 25 points out of a total of 110 (23%) were below**
 394 **the 1:1 line.**

395

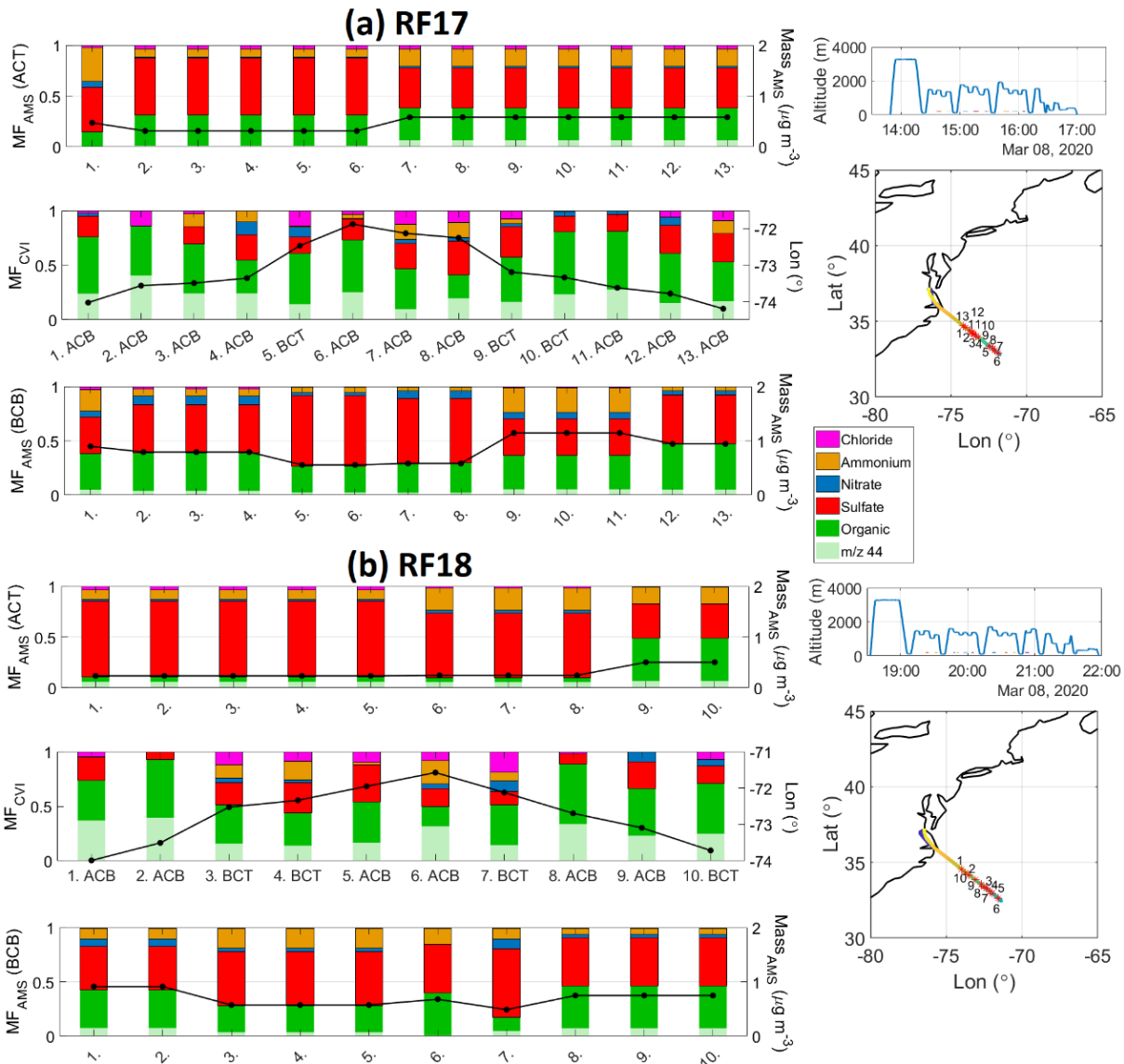
396 The previous discussion does not provide support for any form of artifact or contamination
 397 explaining why 74% of the CVI data points exhibited higher organic mass fractions than both the
 398 BCB or ACT legs. One could argue that the chemical signature of cloud processing should be
 399 evident out of cloud somewhere as ultimately the droplet residual particles will evaporate outside
 400 of cloud and return to the aerosol phase. As will be discussed in Section 4 though, there is a body
 401 of literature pointing to droplet residuals having the strongest signature of cloud processing rather
 402 than below or above cloud. Although difficult to prove with this dataset, a plausible explanation is
 403 that the processed aerosol dilutes into the MBL at a time-scale that is much faster than the
 404 production/evaporation cycle.

405

406 3.3 Cold Air Outbreak Case Studies

407 Owing to interest in the winter season having the strongest aerosol-cloud
408 interactions (Dadashazar et al., 2021a; Painemal et al., 2021), here we examine six case study
409 research flights (RFs) during CAOs to understand the compositional characteristics below, inside,
410 and above clouds. We focus more on the representative day of 8 March 2020 (Figure 9), which
411 included two consecutive flights (RFs 17 and 18) based out of Hampton, Virginia profiling aerosol
412 and cloud properties in CAO conditions. These two flights were investigated in past work showing
413 enhanced new particle formation in ACT legs (Corral et al., 2022) and that entrainment of free
414 tropospheric air dilutes MBL CCN concentrations (Tornow et al., 2022). The other four flights
415 (Figure 10: RFs 5-6 on 22 February 2020; Figure 11: RFs 10-11 on 28 February 2020) exhibited
416 the same general results as those shown for 8 March with higher organic mass fractions and f_{44} in
417 the cloud legs.

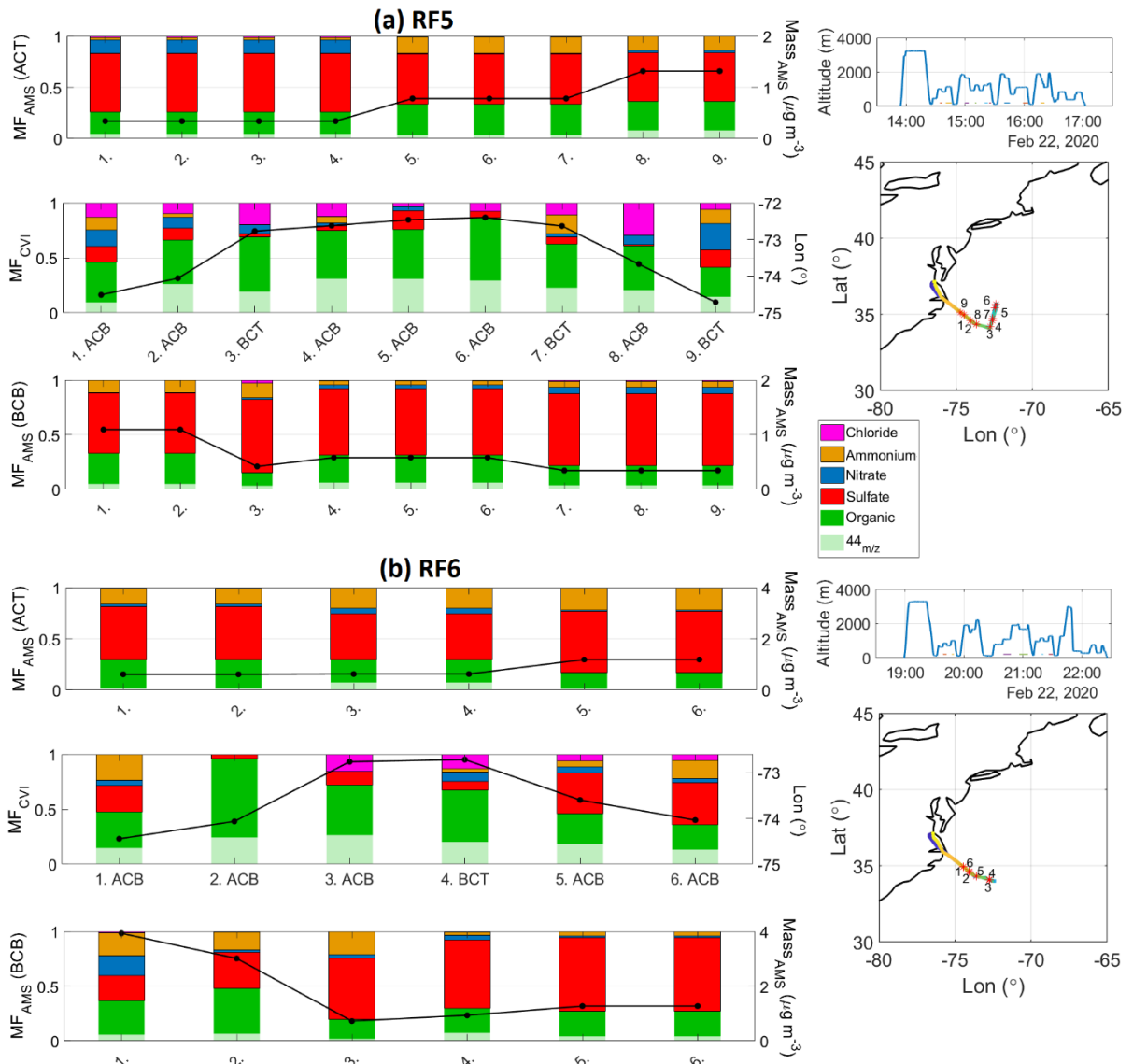
418 Figure 9 shows the AMS composition profile on the out-and-back flights on 8 March,
419 which involved flying out to a point and repeating the same path back to the airfield. Stacked on
420 top of each other in Figure 9 are the corresponding legs within individual cloud ensembles
421 including (from top to bottom) ACT, either BCT or ACB legs with CVI data, and BCB. RF17 in
422 the morning comprised 13 different cloud legs with corresponding BCB and ACT legs. The BCB
423 and ACT mass fraction profiles were similar with sulfate being most abundant (mass fractions:
424 0.34-0.65) followed closely by organics (mass fractions: 0.15-0.42). The f_{44} fraction of the
425 organics in BCB and ACT legs was quite low (0.00-0.16). The cloud data show a very different
426 profile with organics dominating the mass profile (mass fractions: 0.41-0.86) followed usually by
427 sulfate (mass fractions: 0.00-0.30). Furthermore, there was a significant jump in f_{44} in the CVI data
428 (0.21-0.48). RF18 later in the day re-traced the same flight path and included 10 sets of matching
429 cloud-BCB/ACT legs showing again a similar jump in both organic mass fraction and f_{44} in droplet
430 residuals. In the second flight there was more variability in the BCB and ACT pairs, with higher
431 sulfate mass fractions (0.34-0.75) in the ACT legs throughout most of the flight excluding the last
432 two sets of legs. The total AMS mass concentrations were slightly higher in the BCB legs (0.49-
433 0.91 $\mu\text{g m}^{-3}$) relative to ACT legs (0.24-0.50 $\mu\text{g m}^{-3}$).



434

435 **Figure 9. Summary of AMS composition in adjacent BCB, cloud, and ACT legs during back-**
 436 **to-back flights (Research Flights 17 and 18) in CAO conditions on 8 March 2020. Shown in**
 437 **the bar charts are the mass fractions of AMS components in addition to either total AMS**
 438 **mass (for ACT and BCB legs; such data are not robust for CVI legs due to how the CVI**
 439 **operates) or longitude on the right y-axis. Note that some BCB and ACT legs are repeated**
 440 **for different cloud legs as they represent the closest leg to an individual cloud leg. On the far**
 441 **right are Falcon altitude during the flight along with the spatial map with numbers**
 442 **corresponding to the leg set numbers in the bar charts.**

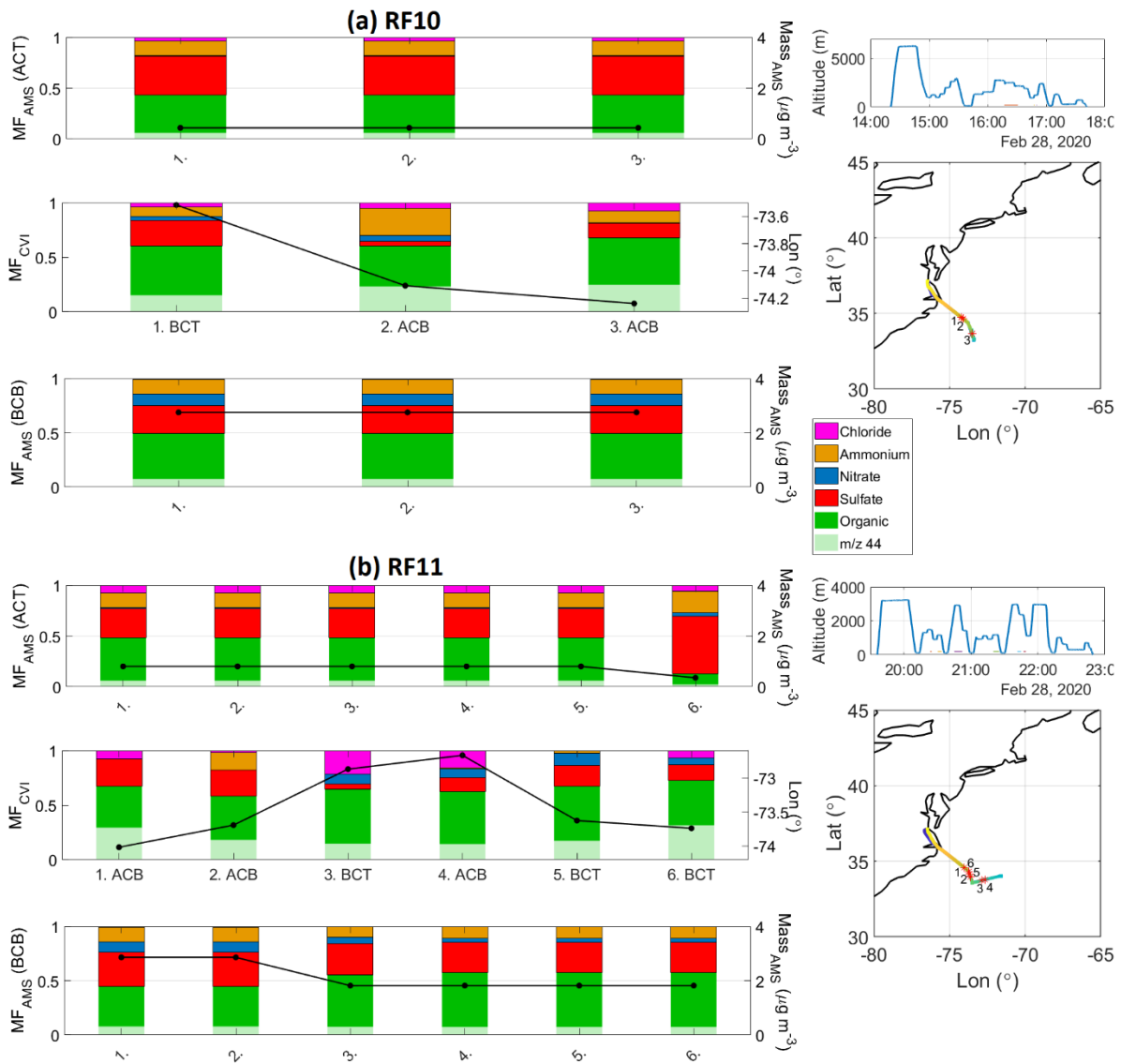
443



444

445 **Figure 10. Summary of AMS composition in adjacent BCB, cloud, and ACT legs during**
 446 **back-to-back flights (Research Flights 5 and 6) in CAO conditions on 22 February 2020.**
 447 **Shown in the bar charts are the mass fractions of AMS components in addition to either**
 448 **total AMS mass (for ACT and BCB legs; such data are not robust for CVI legs due to how**
 449 **the CVI operates) or longitude on the right y-axis. Note that some BCB and ACT legs are**
 450 **repeated for different cloud legs as they represent the closest leg to an individual cloud leg.**
 451 **On the far right are Falcon altitude time series along with the spatial map with numbers**
 452 **corresponding to the leg numbers in the bar charts.**

453



454

455 **Figure 11. Summary of AMS composition in adjacent BCB, cloud, and ACT legs during**
 456 **back-to-back flights (Research Flights 10 and 11) in cold air outbreak conditions on 28**
 457 **February 2020. Shown in the bar charts are the mass fractions of AMS components in**
 458 **addition to either total AMS mass (for ACT and BCB legs; such data are not robust for**
 459 **CVI legs due to how the CVI operates) or longitude on the right y-axis. Note that some**
 460 **BCB and ACT legs are repeated for different cloud legs as they represent the closest leg to**
 461 **an individual cloud leg. On the far right are flight altitude time series along with the spatial**
 462 **map with numbers corresponding to the leg numbers in the bar charts.**

463

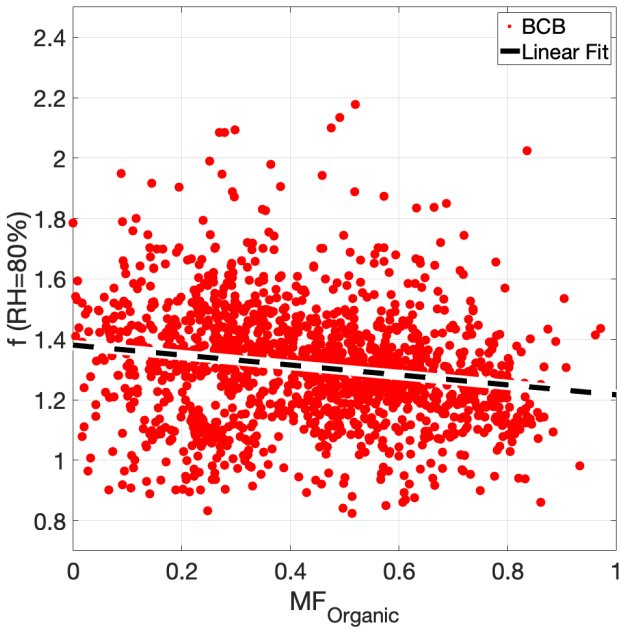
464 **4. Discussion**

465 Our results represent unique atmospheric data that are scarce in the literature owing to the
466 difficulty of obtaining aerosol chemical data below, in, and above cloud in close spatiotemporal
467 proximity across many flights in different times of the year. Figure 1 provides implications of the
468 results in terms of differences with MERRA-2 speciated AOD. Although we cannot
469 unambiguously prove it with the dataset, the results suggest that the most likely explanation for
470 organic and f_{44} enrichment in droplet residuals has to do with aqueous processing rather than
471 preferential activation of CCN with enhanced values of the organic:sulfate ratio and f_{44} . That the
472 droplet residuals shift to a more organic-rich signature with more oxygenated organics has
473 implications for the aerosol particle properties remaining after droplet evaporation as they shift in
474 composition and possibly size. Interestingly this study shows though that such a signature out of
475 cloud was absent for 74% of the cloud cases as organic mass fraction was higher in cloud versus
476 either below or above cloud. These findings are significant in terms of motivating additional
477 research, especially as other studies discussed below also have shown higher levels of organic
478 mass fraction of ratios of oxygenated organics relative to total organic mass in CVI samples as
479 compared to out of cloud.

480 Coggon et al. (2012) showed increased AMS organic:sulfate ratios with altitude in the
481 MBL over the northeast Pacific Ocean coincident with increased liquid water content, which was
482 attributed to aqueous processing effects to generate more organics relative to sulfate; this was also
483 suggested by past work in that region with a PILS (Sorooshian et al., 2007). Coggon et al. (2012)
484 showed that organics and sulfate were typically the most abundant AMS species both below cloud
485 and in droplet residuals with comparable mass fractions and no consistent trend of either one
486 dominating the droplet residual composition; however, they showed that in 70% of their cloud
487 cases that the CVI data exhibited higher organic mass fraction relative to out of cloud. Past
488 measurements off the California coast and over Texas revealed enhanced f_{44} values in droplet
489 residuals relative to below and above cloud data and also relative to interstitial aerosol particles in
490 cloud (Sorooshian et al., 2010). That study showed similarly enhanced values of other ratios in
491 droplet residuals indicative of more oxygenated organics (e.g., PILS oxalate:AMS m/z 44, PILS
492 oxalate:AMS organic). Over the Texas area, PILS measurements of oxalate relative to AMS sulfate
493 and organic revealed significant enhancements (factors up to 4 and 13, respectively) downstream
494 a CVI relative to cloud-free conditions at similar altitudes (Wonaschuetz et al., 2012); furthermore,
495 they showed that organic mass fractions increased together with oxalate:organic and
496 oxalate:sulfate ratios as a function of residual cloud fraction, which was a metric representing
497 “cloud processing history” of an air parcel in shallow cumulus cloud fields. CVI-AMS data from
498 a surface site studying warm tropospheric clouds on Mt. Åreskutan in central Sweden in July 2003
499 showed that organics and nitrate activated with higher ease than sulfate (Drewnick et al., 2007);
500 even though our results suggest the droplet residual changes in composition are likely driven by
501 aqueous processing, it is relevant that organics have been shown in at least one other region to
502 activate more easily than sulfate.

503 While a measurement of hygroscopicity of the droplet residuals was not available, we
504 instead examine aerosol hygroscopicity from BCB legs as that is the area out of cloud most
505 commonly exhibiting higher organic mass fractions relative to in cloud. Even if the signature out
506 of cloud is not as clear as one would expect presumably owing to dilution effects, still the
507 influence of cloud processing on organics inevitably should exist to some extent making the
508 subsequent discussion valuable. Having more organics relative to sulfate may reduce
509 hygroscopicity at high RHs (e.g., Hersey et al., 2009), but a compensating factor could be that

510 the organics are more oxygenated, which would increase the hygroscopicity of the organic
511 fraction itself.



512

513 **Figure 12. Relationship between f(RH) and organic mass fraction for BCB legs during**
514 **ACTIVATE deployments 1-4. Markers are based on f(RH) data synched to the time**
515 **resolution of the AMS data. The f(RH) values from the linear fit at a MF_{organic} value of 0.0**
516 **1.0 are 1.39 and 1.22, respectively.**

517 Figure 12 shows an inverse relationship between f(RH) and organic mass fraction across
518 all the BCB legs in ACTIVATE deployments 1-4, which is similar to what has been observed over
519 the continental U.S. (Shingler et al., 2016); using the linear best fit line shows that the
520 representative f(RH) value for pure organic aerosol (i.e., organic mass fraction of 1.0) was 1.22 in
521 contrast with 0.92 over the continental United States (Shingler et al., 2016). The f(RH) value for
522 pure inorganic aerosol (i.e., organic mass fraction of 0.0) was 1.39. Results of Figure 12 along
523 with previous discussion suggests that aerosol interaction with clouds decreases particle
524 hygroscopicity at an RH of 80% although future work will look deeper into aerosol hygroscopic
525 properties over the ACTIVATE region. This is especially relevant as regulatory activities have
526 reduced sulfate levels over the eastern U.S. in recent decades promoting higher relative amounts
527 of organics (Bates et al., 2005; Hand et al., 2012) with downwind impacts on the northwest Atlantic
528 due to offshore flow (Keene et al., 2014; Aldhaif et al., 2021; Dadashazar et al., 2021b).

529

530 5. Conclusion

531 A large airborne dataset collected over the northwest Atlantic as part of the NASA
532 ACTIVATE mission reveals a distinctly different chemical signature in cloud droplet residuals
533 (lower sulfate mass fraction, higher organic mass fraction, and higher f₄₄) relative to particles
534 below and above cloud for approximately 75% of the cloud cases examined. Several case study
535 flights during cold air outbreak conditions are profiled showing the aforementioned compositional

536 changes in droplet residuals. Detailed analysis suggests this shift in composition is driven more by
537 in-cloud aqueous processing rather than preferential activation of CCN with such chemical
538 characteristics. Of the 29 cases (out of 110) with higher organic mass fraction either above or
539 below clouds versus droplet residuals, 25 (4) exhibited higher organic mass fraction below (above)
540 cloud suggestive of the cloud processing signature being more prevalent below cloud. These
541 results are analogous to past work in other regions using different instrumentation showing
542 maximum values of various metrics relevant to organics (e.g., f_{44} , organic mass fraction)
543 downstream of a CVI in cloud relative to either below or above cloud (Sorooshian et al., 2010;
544 Coggon et al., 2012; Wonaschuetz et al., 2012). More work is needed to continue validating
545 whether aqueous processing is the primary reason for the composition changes and to determine
546 if these results apply to other regions.

547 The results of this study motivate increased attention to both in-cloud formation of
548 oxygenated organics and the composition of particles activating into droplets over the northwest
549 Atlantic. This work has implications for aerosol-cloud interactions in this region as datasets often
550 relied on in the absence of airborne data such as reanalysis data suggest a different story where
551 sulfate is more enhanced than organics year-round (in contrast to the airborne data) (e.g., Braun et
552 al., 2021). The high relative abundance of organics needs more attention, especially in light of the
553 increasing relative amount of species in aerosol particles other than sulfate due to regulatory
554 activities over the U.S. (Hand et al., 2012).

555 *Data Availability.*

556 ACTIVATE Airborne Data:
557 https://doi.org/10.5067/ASDC/ACTIVATE_Aerosol_AircraftInSitu_Falcon_Data_1
558 (NASA/LARC/SD/ASDC, 2020a),
559 https://doi.org/10.5067/ASDC/ACTIVATE_Cloud_AircraftInSitu_Falcon_Data_1
560 (NASA/LARC/SD/ASDC, 2020b), and
561 https://doi.org/10.5067/ASDC/ACTIVATE_MetNav_AircraftInSitu_Falcon_Data_1
562 (NASA/LARC/SD/ASDC, 2020c).

563 *Author contributions.* HD conducted the analysis. AS and HD prepared the manuscript. All authors
564 contributed by providing input and/or participating in airborne data collection.

565 *Competing interests.* The authors declare that they have no conflict of interest.

566 *Acknowledgments.* The work was funded by NASA grant 80NSSC19K0442 in support of
567 ACTIVATE, a NASA Earth Venture Suborbital-3 (EVS-3) investigation funded by NASA's Earth
568 Science Division and managed through the Earth System Science Pathfinder Program Office. CV
569 and SK thank funding by the DFG CRC 301 TP Change and by HGF W2W3-060. We
570 acknowledge use of imagery from the NASA Worldview application
571 (<https://worldview.earthdata.nasa.gov/>), part of the NASA Earth Observing System Data and
572 Information System. We thank pilots and aircraft maintenance personnel of NASA Langley
573 Research Services Directorate for successful execution of ACTIVATE flights.

574

575 **References**

576 Aldhaif, A. M., Lopez, D. H., Dadashazar, H., Painemal, D., Peters, A. J., and Sorooshian, A.: An
577 Aerosol Climatology and Implications for Clouds at a Remote Marine Site: Case Study Over
578 Bermuda, *Journal of Geophysical Research: Atmospheres*, 126, e2020JD034038,
579 <https://doi.org/10.1029/2020JD034038>, 2021.

580 Asa-Awuku, A., Sorooshian, A., Flagan, R. C., Seinfeld, J. H., and Nenes, A.: CCN Properties of
581 Organic Aerosol Collected Below and within Marine Stratocumulus Clouds near Monterey,
582 California, *Atmosphere*, 6, 1590-1607, 2015.

583 Barth, M. C., Rasch, P. J., Kiehl, J. T., Benkovitz, C. M., and Schwartz, S. E.: Sulfur chemistry in
584 the National Center for Atmospheric Research Community Climate Model: Description,
585 evaluation, features, and sensitivity to aqueous chemistry, *Journal of Geophysical Research:*
586 *Atmospheres*, 105, 1387-1415, <https://doi.org/10.1029/1999JD900773>, 2000.

587 Bates, T. S., Quinn, P. K., Coffman, D. J., Johnson, J. E., and Middlebrook, A. M.: Dominance of
588 organic aerosols in the marine boundary layer over the Gulf of Maine during NEAQS 2002 and
589 their role in aerosol light scattering, *J Geophys Res-Atmos*, 110, 2005.

590 Blando, J. D. and Turpin, B. J.: Secondary organic aerosol formation in cloud and fog droplets: a
591 literature evaluation of plausibility, *Atmospheric Environment*, 34, 1623-1632,
592 [https://doi.org/10.1016/S1352-2310\(99\)00392-1](https://doi.org/10.1016/S1352-2310(99)00392-1), 2000.

593 Braun, R. A., McComiskey, A., Tselioudis, G., Trops, D., and Sorooshian, A.: Cloud, Aerosol, and
594 Radiative Properties Over the Western North Atlantic Ocean, *Journal of Geophysical Research:*
595 *Atmospheres*, 126, e2020JD034113, <https://doi.org/10.1029/2020JD034113>, 2021.

596 Coggon, M. M., Sorooshian, A., Wang, Z., Metcalf, A. R., Frossard, A. A., Lin, J. J., Craven, J.
597 S., Nenes, A., Jonsson, H. H., Russell, L. M., Flagan, R. C., and Seinfeld, J. H.: Ship impacts on
598 the marine atmosphere: insights into the contribution of shipping emissions to the properties of
599 marine aerosol and clouds, *Atmos. Chem. Phys.*, 12, 8439-8458, 10.5194/acp-12-8439-2012,
600 2012.

601 Corral, A. F., Braun, R. A., Cairns, B., Gorooh, V. A., Liu, H., Ma, L., Mardi, A. H., Painemal,
602 D., Starnes, S., van Dierenhoven, B., Wang, H., Yang, Y., Zhang, B., and Sorooshian, A.: An
603 Overview of Atmospheric Features Over the Western North Atlantic Ocean and North American
604 East Coast – Part 1: Analysis of Aerosols, Gases, and Wet Deposition Chemistry, *Journal of*
605 *Geophysical Research: Atmospheres*, 126, e2020JD032592,
606 <https://doi.org/10.1029/2020JD032592>, 2021.

607 Corral, A. F., Choi, Y., Crosbie, E., Dadashazar, H., DiGangi, J. P., Diskin, G. S., Fenn, M.,
608 Harper, D. B., Kirschler, S., Liu, H., Moore, R. H., Nowak, J. B., Scarino, A. J., Seaman, S.,
609 Shingler, T., Shook, M. A., Thornhill, K. L., Voigt, C., Zhang, B., Ziemba, L. D., and Sorooshian,
610 A.: Cold Air Outbreaks Promote New Particle Formation Off the U.S. East Coast, *Geophysical*
611 *Research Letters*, 49, e2021GL096073, <https://doi.org/10.1029/2021GL096073>, 2022.

612 Dadashazar, H., Ma, L., and Sorooshian, A.: Sources of pollution and interrelationships between
613 aerosol and precipitation chemistry at a central California site, *Science of The Total Environment*,
614 651, 1776-1787, <https://doi.org/10.1016/j.scitotenv.2018.10.086>, 2019.

615 Dadashazar, H., Painemal, D., Alipanah, M., Brunke, M., Chellappan, S., Corral, A. F., Crosbie,
616 E., Kirschler, S., Liu, H., Moore, R. H., Robinson, C., Scarino, A. J., Shook, M., Sinclair, K.,
617 Thornhill, K. L., Voigt, C., Wang, H., Winstead, E., Zeng, X., Ziemba, L., Zuidema, P., and
618 Sorooshian, A.: Cloud drop number concentrations over the western North Atlantic Ocean:
619 seasonal cycle, aerosol interrelationships, and other influential factors, *Atmos. Chem. Phys.*, 21,
620 10499-10526, 10.5194/acp-21-10499-2021, 2021a.

621 Dadashazar, H., Alipanah, M., Hilario, M. R. A., Crosbie, E., Kirschler, S., Liu, H., Moore, R. H.,
622 Peters, A. J., Scarino, A. J., Shook, M., Thornhill, K. L., Voigt, C., Wang, H., Winstead, E., Zhang,
623 B., Ziemba, L., and Sorooshian, A.: Aerosol responses to precipitation along North American air
624 trajectories arriving at Bermuda, *Atmos. Chem. Phys.*, 21, 16121-16141, 10.5194/acp-21-16121-
625 2021, 2021b.

626 DeCarlo, P. F., Dunlea, E. J., Kimmel, J. R., Aiken, A. C., Sueper, D., Crouse, J., Wennberg, P.
627 O., Emmons, L., Shinozuka, Y., Clarke, A., Zhou, J., Tomlinson, J., Collins, D. R., Knapp, D.,
628 Weinheimer, A. J., Montzka, D. D., Campos, T., and Jimenez, J. L.: Fast airborne aerosol size and

629 chemistry measurements above Mexico City and Central Mexico during the MILAGRO campaign,
630 *Atmos. Chem. Phys.*, 8, 4027-4048, 10.5194/acp-8-4027-2008, 2008.

631 de Gouw, J. A., Middlebrook, A. M., Warneke, C., Goldan, P. D., Kuster, W. C., Roberts, J. M.,
632 Fehsenfeld, F. C., Worsnop, D. R., Canagaratna, M. R., Pszenny, A. A. P., Keene, W. C.,
633 Marchewka, M., Bertman, S. B., and Bates, T. S.: Budget of organic carbon in a polluted
634 atmosphere: Results from the New England Air Quality Study in 2002, *Journal of Geophysical*
635 *Research: Atmospheres*, 110, 10.1029/2004jd005623, 2005.

636 Drewnick, F., Schneider, J., Hings, S. S., Hock, N., Noone, K., Targino, A., Weimer, S., and
637 Borrmann, S.: Measurement of Ambient, Interstitial, and Residual Aerosol Particles on a
638 Mountaintop Site in Central Sweden using an Aerosol Mass Spectrometer and a CVI, *Journal of*
639 *Atmospheric Chemistry*, 56, 1-20, 10.1007/s10874-006-9036-8, 2007.

640 Ervens, B., Turpin, B. J., and Weber, R. J.: Secondary organic aerosol formation in cloud droplets
641 and aqueous particles (aqSOA): a review of laboratory, field and model studies, *Atmos. Chem.*
642 *Phys.*, 11, 11069-11102, 10.5194/acp-11-11069-2011, 2011.

643 Ervens, B.: Modeling the Processing of Aerosol and Trace Gases in Clouds and Fogs, *Chemical*
644 *Reviews*, 115, 4157-4198, 10.1021/cr5005887, 2015.

645 Gelaro, R., McCarty, W., Suárez, M. J., Todling, R., Molod, A., Takacs, L., Randles, C. A.,
646 Darmenov, A., Bosilovich, M. G., Reichle, R., Wargan, K., Coy, L., Cullather, R., Draper, C.,
647 Akella, S., Buchard, V., Conaty, A., da Silva, A. M., Gu, W., Kim, G.-K., Koster, R., Lucchesi,
648 R., Merkova, D., Nielsen, J. E., Partyka, G., Pawson, S., Putman, W., Rienecker, M., Schubert, S.
649 D., Sienkiewicz, M., and Zhao, B.: The Modern-Era Retrospective Analysis for Research and
650 Applications, Version 2 (MERRA-2), *J Clim*, 30, 5419-5454, 10.1175/jcli-d-16-0758.1, 2017.

651 Grosvenor, D. P., Sourdeval, O., Zuidema, P., Ackerman, A., Alexandrov, M. D., Bennartz, R.,
652 Boers, R., Cairns, B., Chiu, J. C., Christensen, M., Deneke, H., Diamond, M., Feingold, G.,
653 Fridlind, A., Hünerbein, A., Knist, C., Kollias, P., Marshak, A., McCoy, D., Merk, D., Painemal,
654 D., Rausch, J., Rosenfeld, D., Russchenberg, H., Seifert, P., Sinclair, K., Stier, P.,
655 van Diedenhoven, B., Wendisch, M., Werner, F., Wood, R., Zhang, Z., and Quaas, J.: Remote
656 Sensing of Droplet Number Concentration in Warm Clouds: A Review of the Current State of
657 Knowledge and Perspectives, *Reviews of Geophysics*, 56, 409-453,
658 <https://doi.org/10.1029/2017RG000593>, 2018.

659 Hand, J. L., Schichtel, B. A., Malm, W. C., and Pitchford, M. L.: Particulate sulfate ion
660 concentration and SO₂ emission trends in the United States from the early 1990s through 2010,
661 *Atmos Chem Phys*, 12, 10353-10365, 2012.

662 Hawkins, L. N., Russell, L. M., Twohy, C. H., and Anderson, J. R.: Uniform particle-droplet
663 partitioning of 18 organic and elemental components measured in and below DYCOMS-II
664 stratocumulus clouds, *Journal of Geophysical Research: Atmospheres*, 113,
665 <https://doi.org/10.1029/2007JD009150>, 2008.

666 Heald, C. L., Coe, H., Jimenez, J. L., Weber, R. J., Bahreini, R., Middlebrook, A. M., Russell, L.
667 M., Jolleys, M., Fu, T. M., Allan, J. D., Bower, K. N., Capes, G., Crosier, J., Morgan, W. T.,
668 Robinson, N. H., Williams, P. I., Cubison, M. J., DeCarlo, P. F., and Dunlea, E. J.: Exploring the
669 vertical profile of atmospheric organic aerosol: comparing 17 aircraft field campaigns with a global
670 model, *Atmos. Chem. Phys.*, 11, 12673-12696, 10.5194/acp-11-12673-2011, 2011.

671 Hegg, D. A., Livingston, J., Hobbs, P. V., Novakov, T., and Russell, P.: Chemical apportionment
672 of aerosol column optical depth off the mid-Atlantic coast of the United States, *J Geophys Res-*
673 *Atmos*, 102, 25293-25303, 1997.

674 Hersey, S. P., Sorooshian, A., Murphy, S. M., Flagan, R. C., and Seinfeld, J. H.: Aerosol
675 hygroscopicity in the marine atmosphere: a closure study using high-time-resolution, multiple-RH
676 DASH-SP and size-resolved C-ToF-AMS data, *Atmos. Chem. Phys.*, 9, 2543-2554, 10.5194/acp-
677 9-2543-2009, 2009.

678 Hilario, M. R. A., Crosbie, E., Bañaga, P. A., Betito, G., Braun, R. A., Cambaliza, M. O., Corral,
679 A. F., Cruz, M. T., Dibb, J. E., Lorenzo, G. R., MacDonald, A. B., Robinson, C. E., Shook, M. A.,
680 Simpas, J. B., Stahl, C., Winstead, E., Ziemba, L. D., and Sorooshian, A.: Particulate Oxalate-To-
681 Sulfate Ratio as an Aqueous Processing Marker: Similarity Across Field Campaigns and
682 Limitations, *Geophysical Research Letters*, 48, e2021GL096520,
683 <https://doi.org/10.1029/2021GL096520>, 2021.

684 Hsu, Y.-K., Holsen, T. M., and Hopke, P. K.: Comparison of hybrid receptor models to locate PCB
685 sources in Chicago, *Atmospheric Environment*, 37, 545-562, [https://doi.org/10.1016/S1352-](https://doi.org/10.1016/S1352-2310(02)00886-5)
686 [2310\(02\)00886-5](https://doi.org/10.1016/S1352-2310(02)00886-5), 2003.

687 Keene, W. C., Moody, J. L., Galloway, J. N., Prospero, J. M., Cooper, O. R., Eckhardt, S., and
688 Maben, J. R.: Long-term trends in aerosol and precipitation composition over the western North
689 Atlantic Ocean at Bermuda, *Atmos Chem Phys*, 14, 8119-8135, 2014.

690 Kirschler, S., Voigt, C., Anderson, B., Campos Braga, R., Chen, G., Corral, A. F., Crosbie, E.,
691 Dadashazar, H., Ferrare, R. F., Hahn, V., Hendricks, J., Kaufmann, S., Moore, R., Pöhlker, M. L.,
692 Robinson, C., Scarino, A. J., Schollmayer, D., Shook, M. A., Thornhill, K. L., Winstead, E.,
693 Ziemba, L. D., and Sorooshian, A.: Seasonal updraft speeds change cloud droplet number
694 concentrations in low level clouds over the Western North Atlantic, *Atmos. Chem. Phys. Discuss.*,
695 2022, 1-32, 10.5194/acp-2022-171, 2022.

696 Lambe, A. T., Onasch, T. B., Massoli, P., Croasdale, D. R., Wright, J. P., Ahern, A. T., Williams,
697 L. R., Worsnop, D. R., Brune, W. H., and Davidovits, P.: Laboratory studies of the chemical
698 composition and cloud condensation nuclei (CCN) activity of secondary organic aerosol (SOA)
699 and oxidized primary organic aerosol (OPOA), *Atmos. Chem. Phys.*, 11, 8913-8928, 10.5194/acp-
700 11-8913-2011, 2011.

701 Leaitch, W. R., Lohmann, U., Russell, L. M., Garrett, T., Shantz, N. C., Toom-Sauntry, D., Strapp,
702 J. W., Hayden, K. L., Marshall, J., Wolde, M., Worsnop, D. R., and Jayne, J. T.: Cloud albedo
703 increase from carbonaceous aerosol, *Atmos Chem Phys*, 10, 7669-7684, 10.5194/acp-10-7669-
704 2010, 2010.

705 Loeb, N. G., Manalo-Smith, N., Su, W., Shankar, M., and Thomas, S.: CERES Top-of-Atmosphere
706 Earth Radiation Budget Climate Data Record: Accounting for in-Orbit Changes in Instrument
707 Calibration, *Remote Sensing*, 8, 182, 2016.

708 Mardi, A. H., Dadashazar, H., Painemal, D., Shingler, T., Seaman, S. T., Fenn, M. A., Hostetler,
709 C. A., and Sorooshian, A.: Biomass Burning Over the United States East Coast and Western North
710 Atlantic Ocean: Implications for Clouds and Air Quality, *Journal of Geophysical Research:*
711 *Atmospheres*, 126, e2021JD034916, <https://doi.org/10.1029/2021JD034916>, 2021.

712 Mertes, S., Verheggen, B., Walter, S., Connolly, P., Ebert, M., Schneider, J., Bower, K. N., Cozic,
713 J., Weinbruch, S., Baltensperger, U., and Weingartner, E.: Counterflow Virtual Impactor Based
714 Collection of Small Ice Particles in Mixed-Phase Clouds for the Physico-Chemical
715 Characterization of Tropospheric Ice Nuclei: Sampler Description and First Case Study, *Aerosol*
716 *Science and Technology*, 41, 848-864, 10.1080/02786820701501881, 2007.

717 Minnis, P., Sun-Mack, S., Young, D. F., Heck, P. W., Garber, D. P., Chen, Y., Spangenberg, D.
718 A., Arduini, R. F., Trepte, Q. Z., Smith, W. L., Ayers, J. K., Gibson, S. C., Miller, W. F., Hong,
719 G., Chakrapani, V., Takano, Y., Liou, K. N., Xie, Y., and Yang, P.: CERES Edition-2 Cloud
720 Property Retrievals Using TRMM VIRS and Terra and Aqua MODIS Data—Part I: Algorithms,
721 *IEEE Transactions on Geoscience and Remote Sensing*, 49, 4374-4400,
722 10.1109/TGRS.2011.2144601, 2011.

723 Minnis, P., Sun-Mack, S., Chen, Y., Chang, F. L., Yost, C. R., Smith, W. L., Heck, P. W., Arduini,
724 R. F., Bedka, S. T., Yi, Y., Hong, G., Jin, Z., Painemal, D., Palikonda, R., Scarino, B. R.,
725 Spangenberg, D. A., Smith, R. A., Trepte, Q. Z., Yang, P., and Xie, Y.: CERES MODIS Cloud
726 Product Retrievals for Edition 4—Part I: Algorithm Changes, *IEEE Transactions on Geoscience*
727 *and Remote Sensing*, 59, 2744-2780, 10.1109/TGRS.2020.3008866, 2021.

728 Nakajima, T., Higurashi, A., Kawamoto, K., and Penner, J. E.: A possible correlation between
729 satellite-derived cloud and aerosol microphysical parameters, *Geophysical Research Letters*, 28,
730 1171-1174, <https://doi.org/10.1029/2000GL012186>, 2001.

731 Ng, N. L., Canagaratna, M. R., Zhang, Q., Jimenez, J. L., Tian, J., Ulbrich, I. M., Kroll, J. H.,
732 Docherty, K. S., Chhabra, P. S., Bahreini, R., Murphy, S. M., Seinfeld, J. H., Hildebrandt, L.,
733 Donahue, N. M., DeCarlo, P. F., Lanz, V. A., Prévôt, A. S. H., Dinar, E., Rudich, Y., and Worsnop,
734 D. R.: Organic aerosol components observed in Northern Hemispheric datasets from Aerosol Mass
735 Spectrometry, *Atmos. Chem. Phys.*, 10, 4625-4641, 10.5194/acp-10-4625-2010, 2010.

736 Ovadnevaite, J., Ceburnis, D., Canagaratna, M., Berresheim, H., Bialek, J., Martucci, G., Worsnop,
737 D. R., and O'Dowd, C.: On the effect of wind speed on submicron sea salt mass concentrations
738 and source fluxes, *Journal of Geophysical Research: Atmospheres*, 117,
739 <https://doi.org/10.1029/2011JD017379>, 2012.

740 Ovadnevaite, J., Ceburnis, D., Leinert, S., Dall'Osto, M., Canagaratna, M., O'Doherty, S.,
741 Berresheim, H., and O'Dowd, C.: Submicron NE Atlantic marine aerosol chemical composition
742 and abundance: Seasonal trends and air mass categorization, *Journal of Geophysical Research:*
743 *Atmospheres*, 119, 11,850-811,863, <https://doi.org/10.1002/2013JD021330>, 2014.

744 Painemal, D., Corral, A. F., Sorooshian, A., Brunke, M. A., Chellappan, S., Afzali Gorooh, V.,
745 Ham, S.-H., O'Neill, L., Smith Jr., W. L., Tselioudis, G., Wang, H., Zeng, X., and Zuidema, P.:
746 An Overview of Atmospheric Features Over the Western North Atlantic Ocean and North
747 American East Coast—Part 2: Circulation, Boundary Layer, and Clouds, *Journal of Geophysical*
748 *Research: Atmospheres*, 126, e2020JD033423, <https://doi.org/10.1029/2020JD033423>, 2021.

749 Papritz, L., Pfahl, S., Sodemann, H., and Wernli, H.: A Climatology of Cold Air Outbreaks and
750 Their Impact on Air–Sea Heat Fluxes in the High-Latitude South Pacific, *J Clim*, 28, 342-364,
751 10.1175/jcli-d-14-00482.1, 2015.

752 Prabhakar, G., Ervens, B., Wang, Z., Maudlin, L. C., Coggon, M. M., Jonsson, H. H., Seinfeld, J.
753 H., and Sorooshian, A.: Sources of nitrate in stratocumulus cloud water: Airborne measurements
754 during the 2011 E-PEACE and 2013 NiCE studies, *Atmospheric Environment*, 97, 166-173,
755 <https://doi.org/10.1016/j.atmosenv.2014.08.019>, 2014.

756 Rolph, G., Stein, A., and Stunder, B.: Real-time Environmental Applications and Display sYstem:
757 READY, *Environmental Modelling & Software*, 95, 210-228,
758 <https://doi.org/10.1016/j.envsoft.2017.06.025>, 2017.

759 Russell, L. M., Noone, K. J., Ferek, R. J., Pockalny, R. A., Flagan, R. C., and Seinfeld, J. H.:
760 Combustion Organic Aerosol as Cloud Condensation Nuclei in Ship Tracks, *Journal of the*
761 *Atmospheric Sciences*, 57, 2591-2606, 10.1175/1520-0469(2000)057<2591:Coaacc>2.0.Co;2,
762 2000.

763 Schroder, J. C., Campuzano-Jost, P., Day, D. A., Shah, V., Larson, K., Sommers, J. M., Sullivan,
764 A. P., Campos, T., Reeves, J. M., Hills, A., Hornbrook, R. S., Blake, N. J., Scheuer, E., Guo, H.,
765 Fibiger, D. L., McDuffie, E. E., Hayes, P. L., Weber, R. J., Dibb, J. E., Apel, E. C., Jaegle, L.,
766 Brown, S. S., Thornton, J. A., and Jimenez, J. L.: Sources and Secondary Production of Organic
767 Aerosols in the Northeastern United States during WINTER, *J Geophys Res-Atmos*, 123, 7771-
768 7796, 2018.

769 Seethala, C., Zuidema, P., Edson, J., Brunke, M., Chen, G., Li, X.-Y., Painemal, D., Robinson, C.,
770 Shingler, T., Shook, M., Sorooshian, A., Thornhill, L., Tornow, F., Wang, H., Zeng, X., and
771 Ziemba, L.: On Assessing ERA5 and MERRA2 Representations of Cold-Air Outbreaks Across
772 the Gulf Stream, *Geophysical Research Letters*, 48, e2021GL094364,
773 <https://doi.org/10.1029/2021GL094364>, 2021.

774 Shah, V., Jaegle, L., Jimenez, J. L., Schroder, J. C., Campuzano-Jost, P., Campos, T. L., Reeves,
775 J. M., Stell, M., Brown, S. S., Lee, B. H., Lopez-Hilfiker, F. D., and Thornton, J. A.: Widespread
776 Pollution From Secondary Sources of Organic Aerosols During Winter in the Northeastern United
777 States, *Geophysical Research Letters*, 46, 2974-2983, 10.1029/2018gl081530, 2019.

778 Shingler, T., Dey, S., Sorooshian, A., Brechtel, F. J., Wang, Z., Metcalf, A., Coggon, M.,
779 Mülmenstädt, J., Russell, L. M., Jonsson, H. H., and Seinfeld, J. H.: Characterisation and airborne
780 deployment of a new counterflow virtual impactor inlet, *Atmos. Meas. Tech.*, 5, 1259-1269,
781 10.5194/amt-5-1259-2012, 2012.

782 Shingler, T., Crosbie, E., Ortega, A., Shiraiwa, M., Zuend, A., Beyersdorf, A., Ziemba, L.,
783 Anderson, B., Thornhill, L., Perring, A. E., Schwarz, J. P., Campazano-Jost, P., Day, D. A.,
784 Jimenez, J. L., Hair, J. W., Mikoviny, T., Wisthaler, A., and Sorooshian, A.: Airborne
785 characterization of subsaturated aerosol hygroscopicity and dry refractive index from the surface
786 to 6.5 km during the SEAC4RS campaign, *Journal of Geophysical Research: Atmospheres*, 121,
787 4188-4210, <https://doi.org/10.1002/2015JD024498>, 2016.

788 Sorooshian, A., Varutbangkul, V., Brechtel, F. J., Ervens, B., Feingold, G., Bahreini, R., Murphy,
789 S. M., Holloway, J. S., Atlas, E. L., Buzorius, G., Jonsson, H., Flagan, R. C., and Seinfeld, J. H.:
790 Oxalic acid in clear and cloudy atmospheres: Analysis of data from International Consortium for
791 Atmospheric Research on Transport and Transformation 2004, *Journal of Geophysical Research:*
792 *Atmospheres*, 111, <https://doi.org/10.1029/2005JD006880>, 2006a.

793 Sorooshian, A., Brechtel, F. J., Ma, Y., Weber, R. J., Corless, A., Flagan, R. C., and Seinfeld, J.
794 H.: Modeling and Characterization of a Particle-into-Liquid Sampler (PILS), *Aerosol Science and*
795 *Technology*, 40, 396-409, [10.1080/02786820600632282](https://doi.org/10.1080/02786820600632282), 2006b.

796 Sorooshian, A., Lu, M.-L., Brechtel, F. J., Jonsson, H., Feingold, G., Flagan, R. C., and Seinfeld,
797 J. H.: On the Source of Organic Acid Aerosol Layers above Clouds, *Environmental Science &*
798 *Technology*, 41, 4647-4654, [10.1021/es0630442](https://doi.org/10.1021/es0630442), 2007.

799 Sorooshian, A., Murphy, S. M., Hersey, S., Bahreini, R., Jonsson, H., Flagan, R. C., and Seinfeld,
800 J. H.: Constraining the contribution of organic acids and AMS m/z 44 to the organic aerosol
801 budget: On the importance of meteorology, aerosol hygroscopicity, and region, *Geophysical*
802 *Research Letters*, 37, <https://doi.org/10.1029/2010GL044951>, 2010.

803 Sorooshian, A., Anderson, B., Bauer, S. E., Braun, R. A., Cairns, B., Crosbie, E., Dadashazar, H.,
804 Diskin, G., Ferrare, R., Flagan, R. C., Hair, J., Hostetler, C., Jonsson, H. H., Kleb, M. M., Liu, H.,
805 MacDonald, A. B., McComiskey, A., Moore, R., Painemal, D., Russell, L. M., Seinfeld, J. H.,
806 Shook, M., Smith, W. L., Jr., Thornhill, K., Tselioudis, G., Wang, H., Zeng, X., Zhang, B., Ziemba,
807 L., and Zuidema, P.: Aerosol-cloud-meteorology interaction airborne field investigations: Using
808 Lessons Learned from the U.S. West Coast in the Design of ACTIVATE off the U.S. East Coast,
809 *Bulletin of the American Meteorological Society*, 100, 1511-1528, [10.1175/bams-d-18-0100.1](https://doi.org/10.1175/bams-d-18-0100.1),
810 2019.

811 Sorooshian, A., Corral, A. F., Braun, R. A., Cairns, B., Crosbie, E., Ferrare, R., Hair, J., Kleb, M.
812 M., Hossein Mardi, A., Maring, H., McComiskey, A., Moore, R., Painemal, D., Scarino, A. J.,
813 Schlosser, J., Shingler, T., Shook, M., Wang, H., Zeng, X., Ziemba, L., and Zuidema, P.:
814 Atmospheric Research Over the Western North Atlantic Ocean Region and North American East
815 Coast: A Review of Past Work and Challenges Ahead, *Journal of Geophysical Research:*
816 *Atmospheres*, 125, e2019JD031626, <https://doi.org/10.1029/2019JD031626>, 2020.

817 Stein, A. F., Draxler, R. R., Rolph, G. D., Stunder, B. J. B., Cohen, M. D., and Ngan, F.: NOAA's
818 hysplit atmospheric transport and dispersion modeling system, 2015.

819 Tai, A. P. K., Mickley, L. J., and Jacob, D. J.: Correlations between fine particulate matter (PM_{2.5})
820 and meteorological variables in the United States: Implications for the sensitivity of PM_{2.5} to

821 climate change, *Atmospheric Environment*, 44, 3976-3984,
822 <https://doi.org/10.1016/j.atmosenv.2010.06.060>, 2010.

823 Twohy, C. H., Anderson, J. R., Toohey, D. W., Andrejczuk, M., Adams, A., Lytle, M., George, R.
824 C., Wood, R., Saide, P., Spak, S., Zuidema, P., and Leon, D.: Impacts of aerosol particles on the
825 microphysical and radiative properties of stratocumulus clouds over the southeast Pacific Ocean,
826 *Atmos. Chem. Phys.*, 13, 2541-2562, 10.5194/acp-13-2541-2013, 2013.

827 Wang, Y. Q., Zhang, X. Y., and Draxler, R. R.: TrajStat: GIS-based software that uses various
828 trajectory statistical analysis methods to identify potential sources from long-term air pollution
829 measurement data, *Environmental Modelling & Software*, 24, 938-939,
830 <https://doi.org/10.1016/j.envsoft.2009.01.004>, 2009.

831 Warneck, P.: In-cloud chemistry opens pathway to the formation of oxalic acid in the marine
832 atmosphere, *Atmospheric Environment*, 37, 2423-2427, [https://doi.org/10.1016/S1352-2310\(03\)00136-5](https://doi.org/10.1016/S1352-2310(03)00136-5), 2003.

834 Wonaschuetz, A., Sorooshian, A., Ervens, B., Chuang, P. Y., Feingold, G., Murphy, S. M., de
835 Gouw, J., Warneke, C., and Jonsson, H. H.: Aerosol and gas re-distribution by shallow cumulus
836 clouds: An investigation using airborne measurements, *Journal of Geophysical Research:*
837 *Atmospheres*, 117, <https://doi.org/10.1029/2012JD018089>, 2012.

838 Yang, Y., Wang, H., Smith, S. J., Zhang, R., Lou, S., Yu, H., Li, C., and Rasch, P. J.: Source
839 Apportionments of Aerosols and Their Direct Radiative Forcing and Long-Term Trends Over
840 Continental United States, *Earth's Future*, 6, 793-808, <https://doi.org/10.1029/2018EF000859>,
841 2018.

842 Ziemba, L. D., Lee Thornhill, K., Ferrare, R., Barrick, J., Beyersdorf, A. J., Chen, G., Crumeyrolle,
843 S. N., Hair, J., Hostetler, C., Hudgins, C., Obland, M., Rogers, R., Scarino, A. J., Winstead, E. L.,
844 and Anderson, B. E.: Airborne observations of aerosol extinction by in situ and remote-sensing
845 techniques: Evaluation of particle hygroscopicity, *Geophysical Research Letters*, 40, 417-422,
846 <https://doi.org/10.1029/2012GL054428>, 2013.

847 Zorn, S. R., Drewnick, F., Schott, M., Hoffmann, T., and Borrmann, S.: Characterization of the
848 South Atlantic marine boundary layer aerosol using an aerodyne aerosol mass spectrometer,
849 *Atmos. Chem. Phys.*, 8, 4711-4728, 10.5194/acp-8-4711-2008, 2008.